AN EXPERIMENTAL STUDY OF THE THICK TURBULENT BOUNDARY LAYER NEAR THE TAIL OF A BODY OF REVOLUTION

by

V. C. Patel, A. Nakayama, and R. Damian

Sponsored by
General Hydromechanics Research Program
of the Naval Ship Systems Command
Naval Ship Research and Development Center
Contract No. N00014-68-A-0196-0002

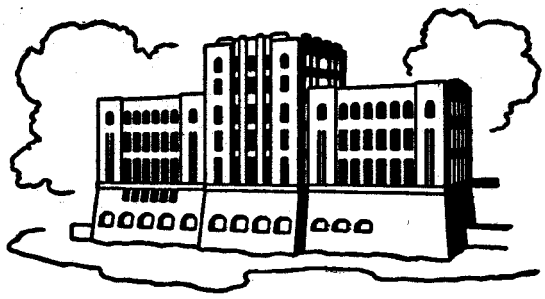

IIHR Report No. 142

Iowa Institute of Hydraulic Research
The University of Iowa
Iowa City, Iowa

January 1973

AN EXPERIMENTAL STUDY OF THE THICK TURBULENT BOUNDARY LAYER NEAR THE TAIL OF A BODY OF REVOLUTION

by

V. C. Patel, A. Nakayama, and R. Damian

Sponsored by
General Hydromechanics Research Program
of the Naval Ship Systems Command
Naval Ship Research and Development Center
Contract No. N00014-68-A-0196-0002

IIHR Report No. 142

Iowa Institute of Hydraulic Research
The University of Iowa
Iowa City, Iowa

January 1973

ABSTRACT

Detailed measurements of pressure distributions, mean velocity profiles and Reynolds stresses were made in the thick axisymmetric turbulent boundary layer near the tail of a body of revolution. The results indicate a number of important differences between the behavior of a thick and a thin boundary layer. The thick boundary layer is characterized by significant variations of static pressure across it and an abnormally low level of turbulence. The static pressure variation is associated with a strong interaction between the boundary layer and the potential flow outside it, while the changes in the turbulence structure appear to be a consequence of the transverse surface curvature. In order to predict the behavior of the flow in the tail region of a body of revolution it is not therefore possible to use conventional thin-boundary-layer calculation procedures.

ACKNOWLEDGEMENTS

The authors wish to thank Professor L. Landweber for introducing them to the problem. The authors also acknowledge the assistance offered by Professor J.R. Glover in the use of hot-wire anemometers, and by Mr. Dale Harris, and his workshop staff, in the construction of the experimental apparatus.

This report is based upon research conducted under the General Hydromechanics Research Program of the Naval Ship Systems Command, technically administered by the Naval Ship Research and Development Center, under Contract N00014-68-A-0196-0002.

LIST OF CONTENTS

LIST OF TABLES

LIST OF FIGURES

AN EXPERIMENTAL STUDY OF THE THICK TURBULENT BOUNDARY LAYER NEAR THE TAIL OF A BODY OF REVOLUTION

I. INTRODUCTION

A number of previous studies have shown that, when the thickness of the boundary layer on a body of revolution becomes of the same order as the local radius of the body, the influence of transverse (or lateral) curvature, which is usually neglected in thin boundary-layer theory, becomes appreciable. Such a situation arises in the case of the boundary layer developing on a long slender cylinder placed axially in a stream. This particular configuration has been examined experimentally and theoretically in some detail in previous investigations. In his recent paper Cebeci (1970) has reviewed the previous studies in both laminar and turbulent boundary layers, and also presented the results of his own calculations using finite-difference techniques. For laminar flow the situation appears to be quite satisfactory insofar as Cebeci's numerical results cover a wide range of conditions and also show substantial agreement with the results of other, not so extensive, analytical studies. In the case of the turbulent boundary layer Cebeci employed an eddy-viscosity model with the additional assumption that this model is not directly affected by transverse curvature. Thus, the influence of curvature is taken into account only in the mean-flow momentum and continuity equations. While the results of these calculations show a plausible effect of transverse curvature, and also agree with the experimental results of Richmond (1957) and Yasuhara (1959), the assumption that the same eddy-viscosity model applies to both thin and thick boundary layers remains to be verified directly since it implies that the turbulent motion itself is not explicitly influenced by transverse curvature. In order to demonstrate the validity of such an assumption it is of course necessary to make detailed turbulence measurements in thick axisymmetric boundary layers. Such measurements have not been reported so far. From the recent study of Patel (1972) it appears that the use of an universal mixing-length or eddy-viscosity model adequately describes the velocity

distribution in the wall region of a thick axisymmetric boundary layer. More experimental data are, however, needed to elucidate the turbulent motion in the outer region.

The cylinder problem cited above is ideally suited for studying the influence of transverse curvature on the development of the boundary layer since the absence of pressure gradients in this case enables one to isolate the curvature effect. In many practical situations, however, significant transverse curvature effects occur in conjunction with streamwise pressure gradients, and possibly with longitudinal surface curvature. Well known examples of this type of flows are the boundary layers in the mid-section of conical and annular diffusers. Another, equally important, case is the flow in the tail region of a body of revolution. In this case the boundary layer over the fore part of the body is thin and can be treated by conventional techniques, but if the body is sufficiently long and slender, the boundary layer in the tail region will grow to a thickness which is comparable with, or even much larger than, the local radius of the body. The present study deals with this latter case. It will be obvious that here we have a case in which both transverse curvature and pressure gradients may dominate the flow. As we shall see later, this flow exhibits several other features of interest: amongst these being a strong interaction between the boundary layer and the potential flow outside it.

This paper describes mean-flow and turbulence measurements in the thick axisymmetric boundary layer on a body of revolution. A parallel theoretical study was undertaken to develop methods for calculating such a thick boundary layer and also to investigate the possibilities of calculating, simultaneously, the potential and boundary-layer flows, allowing the two to interact. The results of these studies will be published separately.

In the literature there are several publications which report measurements on boundary layers in conical diffusers and on bodies of revolution but none of these was made with a view to study the interaction phenomenon just mentioned. Moreover, there is little information concerning the turbulence in a thick axisymmetric boundary layer. In the case of the body of revolution, the interaction is important since the pressure distribution on the surface is modified considerably by the boundary layer even when the flow does not

separate anywhere. The pressure recovery at the tail (or, the pressure variation through the boundary layer at the tail) are obviously needed to obtain better estimates of the total drag experienced by the body. The present experiments were designed specifically to study these aspects of the flow.

II. EXPERIMENTAL ARRANGEMENT AND INSTRUMENTS

A. Wind Tunnel. The experiments were conducted in the largest closed-circuit wind tunnel of the Iowa Institute of Hydraulic Research. The working-section of the tunnel is 24 feet long with a cross-section in the form of a 5-foot octagon provided by throating a 12-foot square approach section. Although the maximum speed attainable in the tunnel is of the order of 90 ft/sec, all the measurements reported here were made at a nominal speed of 40 ft/sec in order to minimize the influence of tunnel vibration.

B. Model, Mountings and Alignment. A six-to-one prolate spheroid, 5 feet long and 10 inches in maximum diameter, used previously by Chevray (1969) to study axisymmetric wakes, and by Satija (1971) to make preliminary investigations of axisymmetric boundary layers, was used in the present experiments. Two rows of cylindrical lucite beads, 1/4 inch long, were attached with a spacing of 1/4 inch at a distance of 3 inches from the nose to ensure early transition of the boundary layer. In order to avoid separation ahead of the tail, Satija modified the original spheroid used by Chevray by truncating it at a section 2 inches from the tail and glueing a conical tail piece such that the slope of the surface remained continuous at the junction. With this modification the overall length of the model became 62.14 inches. The model is shown schematically in Figure 1.

The model was mounted in the wind tunnel by means of eight 0.041 inch diameter steel wires in tension, four at each end of the model. Each wire was provided with a screw-coupling such that its length could be easily adjusted and the model located at any desired position.

In order to obtain axial symmetry of the boundary layer the geometric axis of the model was first aligned with the centerline of the tunnel.

Three identical Pitot tubes, 1/4 inch diameter, were then placed in contact with the surface at an interval of 120 degrees around the body at a section about 2-1/2 inches from the tail. Small adjustments were then made in the lengths of the supporting wires until the total pressures recorded by the three tubes became equal. This procedure was repeated by placing three similar tubes at about the mid-section of the model. Finally, six Pitot tubes were used, three at each of the two sections, the tubes downstream being offset by 60 degrees relative to those upstream. Only minor adjustments were required in this final stage to obtain agreement between the readings of the three tubes at each section. Since the readings of the Pitot tubes may be regarded as a measure of the wall shear stress, and consequently of the velocity distribution in the wall region, this procedure ensured axial symmetry of the flow.

As an additional check on the axial symmetry, the axial components of mean and fluctuating velocities were measured by means of a hot-wire anemometer in the wake of the body 3 inches downstream from the tail. Although the measurements were made in only one plane across the wake, the distributions of mean velocity and the root-mean-square values of the fluctuating velocity were found to be closely symmetrical about the geometric axis of the model. From these measurements it was concluded that the boundary layer on the model was axially symmetric to a sufficient degree of accuracy.

C. Traversing Mechanism. The essential features of the traverse mechanism used in the experiments are shown in Figure 1. The mechanism consisted of a rigid rod with three degrees of freedom in the horizontal plane passing through the axis of the model: transverse motion along the length of the rod, transverse motion along a slide situated outside the tunnel, and rotation about a pivot on this slide. The mechanism was thus capable of traversing measuring probes, such as Pitot tubes and hot-wire probes, mounted on the end of the rod by suitable brackets, in the direction normal to the model surface at a number of discrete streamwise locations on the model. The length of the slide was such that the most upstream point on the model which could be investigated was about 66 percent of the model length from the nose. For the purpose of the present study this was considered quite adequate. At

the other end, measurements could be made right up to the tail of the model. The main rod of the traverse mechanism was provided with a screw drive, a scale and a vernier so that the normal distance of the probes from the model surface could be adjusted and measured from outside the tunnel with a resolution of 0.001 foot. The rod entered the tunnel through a narrow slit cut out of the tunnel wall. The portion of the slit not occupied by the rod was sealed by a rubber sheet to prevent any leakage of air from the tunnel.

The traversing rod had to be made rigid enough to prevent it from vibrating in the wind. In order to minimize the interference between the traversing mechanism and the flow being measured the probes were attached such that the distance between the probe tip and the traversing rod was as large as possible.

D. Measuring Instruments. All total (Pitot) and static pressures were measured using probes of standard design, made from hypodermic tubing of outside diameters 0.050 inch and 0.065 inch respectively, in conjunction with micro-manometers capable of resolving pressure differences of the order of 0.001 inch alcohol The air temperature and pressure in the tunnel were measured immediately downstream of the contraction. These, together with the barometric pressure and dry- and wet-bulb temperatures in the laboratory, were used to find the density and viscosity of the air as well as to correct the manometer readings in the manner suggested by Naudascher (1964).

Mean velocities and the Reynolds stresses within the boundary layer on the model were measured by means of single- and cross-wire probes using the two-channel, constant-temperature, "Old Gold Model, Type 4-2H Hot-Wire Anemometer" and "Type 2 Mean-Product Computer", designed and manufactured by the Iowa Institute of Hydraulic Research. These instruments are built with all solid-state electronic components and equipped with a linearizing circuit for each hot-wire channel and an analog-to-frequency converter. Other features of the design and principles of operation of this anemometer system have been described by Glover (1972). The single-wire and cross-wire probes used in the measurement of mean and fluctuating velocity components were all made from copper-plated tungsten wires of nominal diameter 0.000113 inch and resistance 2570 ohms/foot.

Preliminary experiments conducted at the beginning of the present study, as well as those made earlier by Satija, indicated an unrealistically low level of turbulence in the boundary layer on the spheroidal model. After a considerable amount of experimentation, the origin of this anamoly was traced to an inadequate frequency response of the hot-wire anemometer. Once this was discovered, modifications were made in the amplifier circuits to improve the frequency response and at the same time to cut down the noise level. The necessary modifications were relatively minor. In order to ensure that the modified system performed adequately, a number of tests were conducted in fully-developed turbulent pipe flow. A 2-inch diameter, 30 feet long copper pipe was constructed for this purpose. Measurements with Pitot tubes, and single-wire and cross-wire probes, were then made a few inches upstream of the pipe exit, and the results compared with those of Laufer (1954). Satisfactory agreement was obtained with the data of Laufer as regards the distributions across the pipe of mean velocity, the Reynolds shear stress and the turbulent normal stresses (i.e. the mean-square values of the three components of velocity fluctuation).

In addition to providing a check on the performance of the hot-wire anemometer, the pipe experiments also served to highlight the problems, such as drift in the calibration curves and the necessity to have identical calibration curves for both wires in cross-wire operation, associated with the use of the instruments. These tests also suggested the techniques to be followed in subsequent experiments in order to obtain reliable and consistent data.

III. SOME OBSERVATIONS FROM PRELIMINARY EXPERIMENTS

Exploratory measurements in the boundary layer on the spheroidal model were first made by traversing the total-head and static-pressure tubes separately across the boundary layer at a number of streamwise stations ranging from about 66 percent of model length to the tail. Both tubes were oriented parallel to the model surface. These measurements indicated, amongst other things, that the boundary layer remained attached right up to the tail and that

large variations of static pressure occurred across the boundary layer over the last 10 percent of the model length. This variation in static pressure was accompanied by a dramatic increase in the thickness of the boundary layer.

Before describing the detailed measurements which were made later on, it is convenient to discuss briefly the consequences of these early observations. The rapid thickening of the boundary layer and the large variations in the static pressure in the direction normal to the body surface of course indicated that the mean-flow streamlines within the boundary layer did remain closely parallel to the surface. Alternatively, the component of velocity normal to the wall could no longer be assumed to be an order of magnitude smaller than the component parallel to the wall, as is the case in thin boundary layers. A number of important conclusions pertaining to the measuring techniques follow immediately:

(i) Since the direction of the mean-flow streamlines change continuously across the boundary layer, a simple static-pressure probe, mounted parallel to the body surface, cannot be relied upon to give an accurate measure of the local static pressure, especially at large distances from the surface. If such a probe is to be used with any success its orientation must be changed continuously to coincide with the local streamline direction, which is not known a priori.

(ii) A properly designed total-head tube can be made insensitive to yaw angles up to 30 degrees so that it can be used in the present situation without incurring appreciable errors.

(iii) Owing to the difficulty of measuring static pressure mentioned above, the Pitot-static combination cannot be used to measure the velocity distribution across the boundary layer.

(iv) In order to measure the velocity profiles in the tail region it is therefore necessary to use hot-wire techniques. A single hot-wire probe, traversed normal to the body surface will, however, give the distribution of the resultant velocity through the boundary layer but not the angle which the velocity vector makes with the surface of the body.

(v) The variation of static pressure through the boundary layer

can in principle be determined by taking the difference between the total-head measured by a Pitot tube and the dynamic pressure recorded by means of a single wire. As we shall see later, this procedure is not altogether satisfactory, although consistent results can be obtained when due care is taken.

(vi) To specify the velocity field in the tail region of the body completely, it is necessary to measure the components of mean velocity along and normal to the body surface. This can best be accomplished by traversing a cross-wire probe in the direction normal to the surface.

(vii) The use of cross-wire probes to measure mean velocities has the additional advantage that the Reynolds normal and shear stresses can also be measured at the same time.

The above conclusions contributed in large measure to the final procedures adopted for making the measurements reported below. Traverses of total-head and static-pressure tubes, and single-wire and cross-wire probes, were made at seven streamwise stations on the model, namely X/L = 0.662, 0.80, 0.85, 0.90, 0.93, 0.96 and 0.99, where X denotes the distance from the nose of the model measured along the axis and L the overall length (= 62.14 inches) of the model. All measurements were made at a nominal unit Reynolds number of 2.44×10^5 per foot.

The relative positions of the seven measuring stations and the notation adopted for the presentation of data are shown in Figure 2. The complete model is described by the radius distribution

$$\frac{r_o}{L} = \frac{1}{6}\left\{\frac{X}{L}\left(0.9655 - \frac{X}{L}\right)\right\}^{\frac{1}{2}}, \quad 0 < \frac{X}{L} < 0.9333$$

and

$$\frac{r_o}{L} = 0.4333\left(1 - \frac{X}{L}\right), \quad 0.9333 < \frac{X}{L} < 1.000 \ .$$

The angle between the tangent to the surface and the axis of the model is ϕ. x and y are curvilinear coordinates measured along and normal to the surface, respectively. If r is the distance of a point from the model axis, it follows that

$$r = r_o + y \cos \phi \ .$$

The components of mean velocity along x and y are U and V, respectively. The resultant velocity at any point is denoted by Q, so that $Q = (U^2 + V^2)^{\frac{1}{2}}$. The velocity fluctuations will be denoted by lower-case letters. In addition to these, we have the total pressure P, the static pressure p, density ρ, and kinematic viscosity ν. Subscripts w and δ will be used to signify values at the wall (y=0) and at the edge of the boundary layer ($y=\delta$), respectively.

IV. MEAN FLOW MEASUREMENTS

The total-head (Pitot) tube described earlier was first tested for insensitivity to yaw and then traversed through the boundary layer, keeping it parallel to the body surface, at each of the seven streamwise measuring stations. The total pressure was referenced to the static pressure (p_{ref}) in the tunnel just downstream from the contraction and made dimensionless by dividing by the tunnel dynamic pressure ($\frac{1}{2}\rho U_{ref}^2$) which was held constant in all tests. The measured variations of the total-pressure coefficient, $C_P = (P-p_{ref})/\frac{1}{2}\rho U_{ref}^2$, are shown in Figure 3. Since C_P becomes constant with y outside the boundary layer, these measurements were used to estimate the boundary layer thickness δ. The variation of δ and the ratio δ/r_o, with streamwise distance is shown in Figure 4.

Similar measurements were then made using the static-pressure tube and again the data were rendered dimensionless using the same reference conditions as before. The variations of the static-pressure coefficient, $C_p = (p-p_{ref})/\frac{1}{2}\rho U_{ref}^2$, are also shown in Figure 3. As indicated in the last section, these static pressure measurements may be suspect in the outer regions of the boundary layer over the last 10 percent of the length of the model due to the yaw sensitivity of the probe. They are, however, included here for comparison with results obtained by an alternative method. Since the measurements close to the wall are not in doubt even up to the tail (the flow being locally parallel to the wall), the streamwise variation of static pressure on the model surface, C_{p_w}, was determined by extrapolating the measurements to the wall. A plot of C_{p_w} versus X/L is made in Figure 5,

from which it will be seen that the pressure gradient on the wall is adverse all the way from the first measuring station to the tail. The variation of static pressure at the edge of the boundary layer, $C_{p\delta}$, indicated by the static probe, aligned with the model surface, is also shown in Figure 5. Although the accuracy of the results for X/L greater than 0.93 may be questionable, the figure indicates clearly the large static pressure variations across the boundary layer near the tail of the model. The other results shown in Figure 5 are described later on.

From the total and static pressure distributions described above, it was possible to calculate the profiles of total velocity, i.e., Q/Q_δ. These are shown in Figure 6.

A single hot-wire probe was then traversed through the boundary layer at each of the seven streamwise stations. The wire was held normal to the flow and parallel to the model surface. In these, as well as other hot-wire measurements, care was taken to ensure that the drift of the wire calibration curve was small. Those runs in which the calibration drifted by unduly large amounts were repeated. The profiles of total velocity measured by means of the single wire are compared with those obtained from the Pitot-static measurements in Figure 6. The values of Q_δ, the velocity at the edge of the boundary layer, recorded by the single-wire probe are shown in Figure 5. Also shown in this figure is the pressure variation along the edge of the boundary layer, $C_{p\delta}$, implied by the measured values of Q_δ and the constancy of total pressure.

As mentioned in the last section, the total-pressure profiles measured by the Pitot tube (shown in Figure 3) and the total velocity profiles measured by the single-wire probe were used to infer the static pressure distributions through the boundary layer. The results of this exercise were not altogether satisfactory primarily due to the fact that the static pressure came out as a small difference between two relatively large quantities, neither of which could be measured with the required accuracy. Some consistency was, however, obtained by smoothing the data before taking the differences. The resulting distributions of static pressure are compared with those measured by means of the static-pressure tube in Figures 3 and 5.

In order to determine the components of mean velocity, U and V, along and normal to the model surface, respectively, a cross-wire probe was traversed across the boundary layer at each of the seven measuring stations. A probe with the proper geometric and calibration characteristics was built after several trials. The wires were located in the plane normal to the surface and the flow. The results of the cross-wire measurements were converted to profiles of U/Q_δ, V/Q_δ and Q/Q_δ. These profiles are also shown in Figure 6.

Finally, a preston tube of outside diameter 0.1224 inch was used, in conjunction with the calibration curve of Patel (1965) to determine the wall shear stress, τ_w. A plot of the skin-friction coefficient, $C_f = \tau_w/\frac{1}{2}\rho Q_\delta^2$, is made in Figure 7.

V. ANALYSIS OF THE MEAN-FLOW MEASUREMENTS

A. Boundary Layer Growth. From the variation of boundary layer thickness shown in Figure 4 it is clear that up to about 85 percent of the body length the boundary layer may be regarded as thin insofar as δ is much smaller than r_o, the local radius of the body. Over the last 15 percent of the body length, however, thin boundary-layer theory will cease to apply and transverse curvature effects are expected to play a dominant role in the behavior of the flow.

B. Static-Pressure Distribution. Although, as indicated earlier, the static pressure distributions obtained by the two methods may be suspect as far as accuracy in the tail region of the body is concerned, the results shown in Figures 3 and 5 confirm the observation made above. The static pressure remains substantially constant through the boundary layer right up to X/L = 0.90. From Figure 5 we see that up to this point the pressure at the edge of the boundary layer is somewhat larger than that at the wall. In addition to the well known influence of the normal Reynolds stress $\overline{v^2}$, this increase in pressure with distance from the wall may partly be attributed to the convex curvature of the mean-flow streamlines associated with the convex longitudinal curvature of the body surface.

The decrease in static pressure from the wall towards the edge of the boundary layer in the tail region of the body ($X/L > 0.90$), on the other hand, appears to be a consequence of the concave curvature of the mean-flow streamlines associated primarily with the rapid thickening of the boundary layer. The change from the thin to the thick boundary layer behavior seems to take place in the region of the $X/L = 0.90$ station where δ/r_o is approximately 0.62.

The rapid increase in the thickness of the boundary layer near the tail of the body may of course be regarded as a direct consequence of the ever increasing influence of transverse curvature, but the large variation in static pressure across the boundary layer associated with this thickening suggests that there is a strong interaction between the boundary layer flow and the potential flow outside it. Owing to the presence of the thick boundary layer, potential flow theories can no longer be expected to predict the pressure field in the tail region correctly. At the same time, it is unlikely that usual thin boundary-layer theory, which assumes constant static pressure in the direction normal to the surface, can adequately predict the boundary layer behavior even when the experimentally determined wall pressure distribution is prescribed. Thus, it appears that any rational theory describing the flow in the tail region of a body of revolution with a thick boundary layer must attempt to solve the potential flow and the boundary layer flow simultaneously.

C. Velocity Distributions. Referring to Figure 6, it will be seen that the profiles of the total velocity, Q/Q_δ, measured by the three different methods, namely Pitot and static tubes, single hot-wire, and cross-wire probes, are in reasonable agreement at all streamwise stations. Although we had expected to observe systematic differences between the Pitot-static and the hot-wire results in the outer parts of the boundary layer near the tail of the body, owing to the yaw sensitivity of the static-pressure tube, Figure 6 indicates that any differences which may exist are swamped by the general scatter of the data. Detailed calculations indicated that the expected differences were too small to be distinguished from experimental scatter since the errors incurred in the measurement of static pressure were themselves much smaller than the dynamic pressures from which the total velocities

were calculated. The agreement between the results of three different instruments in a complex flow situation such as this was considered very encouraging.

The profiles of the longitudinal and normal components of mean velocity measured by means of the cross-wire probe clearly show the difference between the thin and the thick boundary layer. Up to X/L = 0.90 the normal component of velocity is seen to be small compared with the longitudinal component, as required in thin boundary-layer theory. By X/L = 0.99, however, the normal component of velocity is almost 32 percent of the longitudinal component at the edge of the boundary layer. Apart from indicating the breakdown of the usual thin boundary-layer assumptions in the tail region, these results confirm the observation made earlier regarding the rapid divergence of the mean-flow streamlines in planes normal to the surface. Indeed, the angle between the surface and the streamline passing through $y = \delta$ at X/L = 0.99 is $\tan^{-1}0.32 = 18.0$ degrees. Since the angle between the tangent to the body surface at this point and the body axis is $\cos^{-1} 0.92 = 23°$, this indicates that the flow near the edge of the boundary layer is more nearly parallel to the axis than the body surface.

The general shape of the velocity profile at the last measuring station shows that the flow there is close to separation. The profile at the most upstream station, X/L = 0.662, was found to conform well with the two-parameter velocity-profile family of Thompson (1965) indicating that the boundary layer there has essentially the same characteristics as one developing on a plane two-dimensional surface.

D. The Mean-Flow Streamlines. The longitudinal components of velocity measured by means of the cross-wire probe, namely U, were used to compute the distributions of the stream function, ψ, at each streamwise measuring station, using the definition:

$$\psi(y) = \int_0^y Ur\, dy = \int_0^y U(r_o + y \cos \phi)dy.$$

Figure 8 shows the mean-flow streamlines within the boundary layer determined from these distributions of ψ. It will be seen that the streamlines are convex and nearly parallel to the surface in the region $0.662 < X/L < 0.90$,

where the boundary layer is thin, and concave and divergent over the last 10 percent of the body length. Figure 8 thus verifies directly the observations made in section V-B simply on the basis of static pressure variations. The angles between the streamlines and the body surface obtained from Figure 8 were found to be in good agreement with those deduced from the direct measurements of the normal and longitudinal components of velocity. This may be regarded as a check on the axial symmetry of the boundary layer.

Figure 8 shows yet another interesting feature of the thick boundary layer near the tail. From the near coincidence of the edge of the boundary layer with a mean-flow streamline it may be concluded that the entrainment of free-stream fluid into the thick boundary layer is small.

E. Integral Parameters from Velocity Profiles. The thickness of the boundary layer at each measuring station was determined from the total-pressure profiles measured by means of the Pitot tube. Thus, δ was defined as the normal distance from the wall where the total pressure became 0.99 times the constant value in the free-stream. This definition appears to be the most appropriate one here for two reasons. First, it gives a unique value of δ even when the static pressure, and therefore the velocity, vary with distance from the wall outside the boundary layer. Secondly, it reduces to the usual definition of δ, as being the distance where the local velocity is 0.995 times the free-stream velocity, when the boundary layer is thin and the static pressure substantially constant across it.

For an axisymmetric boundary layer there appear to be a number of different ways of defining integral parameters such as the displacement and momentum thicknesses.

Perhaps the most meaningful definitions are the physical definitions:

$$\int_{r_o}^{r_o+\delta_1^* \cos\phi} 2\pi r\rho U_p\,dr = \int_{r_o}^{r_o+\delta\cos\phi} 2\pi r\rho(U_p-U)\,dr \qquad (1)$$

and

$$\int_{r_o}^{r_o+\delta_2^* \cos\phi} 2\pi r\rho U_p^2\,dr = \int_{r_o}^{r_o+\delta\cos\phi} 2\pi r\rho U(U_p-U)\,dr, \qquad (2)$$

where U_p is the velocity distribution if the flow were potential right up to the wall, δ_1^* is the physical mass-flux deficit thickness, δ_2^* is the momentum-flux deficit thickness and, as noted before, $r = r_o + y \cos \phi$. The shape factor of the velocity profile and the momentum-thickness Reynolds number of the boundary layer may then be defined as

$$H^* = \frac{\delta_1^*}{\delta_2^*} \quad \text{and} \quad R_\theta^* = \frac{Q_\delta \delta_2^*}{\nu} , \tag{3}$$

respectively. The displacement thickness defined in this manner gives the physical displacement of the external flow streamlines due to the presence of the boundary layer, while the momentum thickness is closely related to the drag experienced by the body. The evaluation of these thicknesses from measured velocity profiles is, however, made difficult by the fact that nothing is known about the variation of the velocity distribution U_p in the hypothetical potential flow over the distance occupied by the boundary layer. If it is assumed that U_p remains constant, and equal to U_δ, over this distance, then equations (1) and (2) simplify to yield

$$\delta_1^*\left(1 + \frac{1}{2}\frac{\delta_1^*}{r_o}\cos\phi\right) = \int_o^\delta \left(1 - \frac{U}{U_\delta}\right)\frac{r}{r_o}\,dy \tag{4}$$

and

$$\delta_2^*\left(1 + \frac{1}{2}\frac{\delta_2^*}{r_o}\cos\phi\right) = \int_o^\delta \frac{U}{U_\delta}\left(1 - \frac{U}{U_\delta}\right)\frac{r}{r_o}\,dy . \tag{5}$$

If the axisymmetric boundary-layer equations are integrated across the layer in the usual manner to obtain the momentum-integral equation, it is found that the integrals on the right-hand-side of equations (4) and (5) arise quite naturally. In almost all previous studies of axisymmetric boundary layers, therefore, the displacement and momentum thicknesses have been defined simply as

$$\delta_1 = \int_o^\delta \left(1 - \frac{U}{U_\delta}\right)\frac{r}{r_o}\,dy \tag{6}$$

and

$$\delta_2 = \int_o^\delta \frac{U}{U_\delta}\left(1 - \frac{U}{U_\delta}\right)\frac{r}{r_o}\,dy , \tag{7}$$

so that

$$H = \frac{\delta_1}{\delta_2} \quad \text{and} \quad R_\theta = \frac{Q_\delta \delta_2}{\nu} \ . \tag{8}$$

We shall refer to these as the usual axisymmetric definitions. A major advantage of using these is that they enable the momentum-integral equation for axisymmetric flow to be written in a form that is simple and very similar to that for plane-surface boundary layers. As we shall see later, however, these definitions lead to some anamolies when the boundary layer is thick in comparison with the local radius of the body. From the expressions given above it will be clear that the usual axisymmetric definitions are related to the physical definitions (using $U_p \simeq U_\delta$) by the formulae

$$\delta_1 = \delta_1^* \left(1 + \frac{1}{2} \frac{\delta_1^*}{r_o} \cos \phi\right) \tag{9}$$

and

$$\delta_2 = \delta_2^* \left(1 + \frac{1}{2} \frac{\delta_2^*}{r_o} \cos \phi\right) \ . \tag{10}$$

Finally, if one is interested only in describing the shape of the velocity profiles, without regard to the geometry of the surface, one can determine the thicknesses using the usual definitions:

$$\bar{\delta}_1 = \int_o^\delta \left(1 - \frac{U}{U_\delta}\right) dy \ , \tag{11}$$

$$\bar{\delta}_2 = \int_o^\delta \frac{U}{U_\delta} \left(1 - \frac{U}{U_\delta}\right) dy \ , \tag{12}$$

$$\bar{H} = \frac{\bar{\delta}_1}{\bar{\delta}_2} \ , \quad \text{and} \quad \bar{R}_\theta = \frac{Q_\delta \bar{\delta}_2}{\nu} \ . \tag{13}$$

We shall refer to these as the planar definitions for obvious reasons.

It will be clear that the physical definitions as well as the usual axisymmetric definitions reduce to the planar definitions given above when the boundary layer is thin, i.e. when $\delta << r_o$. For thick boundary layers, however, the numerical values of the various integral parameters calculated using the three definitions are considerably different.

For the present experiments the integral parameters were calculated

at each streamwise station using all three definitions given above. In the calculation of the thicknesses given by the physical definitions, however, the assumption of $U_p \approx U_\delta$ was not used. Instead, use was made of the distribution of U_p implied by the constancy of total pressure and the observed variation of static pressure, since this would appear to represent the true variation of U_p more realistically. The difference between the values calculated in this manner and those obtained using equations (9) and (10) was found to be of the order of a few percent. Since the profiles of U/U_δ and Q/Q_δ were not substantially different at the first three measuring stations, namely $X/L = 0.662$, 0.80 and 0.85, it was decided to use for these the values of Q/Q_δ indicated by the Pitot and static tubes so as to minimize the influence of the scatter in the hot-wire data. For the last four measuring stations, however, the profiles of U/U_δ recorded by the cross-wire probe were used. The results of these calculations are presented in Figures 9 and 10.

From Figure 9 we see that the nearness to separation at the tail of the body is indicated only by the large value of the shape parameter, $\bar{H}$, which is based solely on the shape of the velocity profile. The other two definitions do not convey this important information. Examination of Figure 10 indicates the large differences in the numerical values of the momentum thickness resulting from the three alternative definitions. It is interesting to note that, when the boundary layer is much thicker than the local radius of the body (e.g. at $X/L = 0.99$), the usual axisymmetric definitions lead to the rather incongruous situation where the momentum and displacement thicknesses become larger than the physical thickness of the boundary layer. (This is of course due to the ever-increasing factor $1/r_o$ appearing in the definitions.) Considerable care may therefore be required in choosing the most meaningful and appropriate definitions of the integral parameters when attempts are made to extend some of the more successful integral calculation methods to treat thick axisymmetric boundary layers.

F. Wall Shear-Stress. The values of the wall shear-stress, measured directly by means of Preston tubes, are compared in Figure 7 with those obtained by applying the method of Clauser (1956) to the profiles of longitudinal velocity, U/U_δ. Also shown in the figure is the variation of C_f obtained from the formula of Thompson (1965) using the measured

values of the planar parameters $\bar{H}$ and $\bar{R}_\theta$. The disagreement between this formula and the Preston-tube and Clauser-plot results appears to imply that the well known two-parameter representation of velocity profiles, upon which the skin-friction formula of Thompson is based, may not adequately describe the velocity profiles in thick axisymmetric boundary layers. This observation was indeed confirmed by detailed comparisons of the measured profiles with Thompson's profile family. It may be remarked here that the use of integral parameters other than those obtained from the planar definitions will not lead to improved correlation between experiment and skin-friction and velocity profile relations commonly used in thin boundary-layer analysis.

VI. MEASUREMENTS OF THE REYNOLDS STRESSES

In the present experiments the Reynolds stresses $\overline{uw}$ and $\overline{vw}$ were assumed to be identically zero on account of the axial symmetry. The remaining components of the Reynolds stress tensor, namely $\overline{u^2}$, $\overline{v^2}$, $\overline{w^2}$ and $\overline{uv}$, were measured by means of cross-wire probes. The results were made dimensionless using the velocity at the edge of the boundary layer and are shown in Figures 11 through 14.

The well known turbulence measurements of Klebanoff (1955) in a flat-plate boundary layer are compared with the present measurements at the most upstream station, X/L = 0.662, in Figure 15. The small disagreement between the two sets of data may be attributed largely to the small adverse pressure gradient which exists at this station and the uncertainties associated with the determination of boundary layer thickness. Nevertheless, the trends shown in Figure 15 indicate that the boundary layer at the most upstream measuring station has the properties of a fully-developed, thin, turbulent boundary layer.

Perhaps the most striking characteristic of the data shown in Figures 11 through 14 is the generally low level of turbulence in the thick boundary layer near the tail of the body. In a thin boundary layer that is proceeding

towards separation the velocity fluctuations and the shear stresses are much larger than those observed here. From the measurements of shear stress and mean velocities the distributions of mixing length and eddy kinematic viscosity were determined using the usual relations

$$-\overline{uv} = L^2\left(\frac{\partial U}{\partial y}\right)^2 \quad , \quad -\overline{uv} = \varepsilon \frac{\partial U}{\partial y} \quad . \tag{14}$$

These are shown in Figures 16 and 17. It may be remarked here that the variations of mixing length were also found using an axisymmetric definition in the form

$$-\overline{uv} = L_A^2 \left\{\frac{1}{r}\frac{\partial}{\partial y}(Ur)\right\}^2 . \tag{15}$$

The values of L_A determined in this manner were found to be substantially lower than those shown in Figure 16, especially near the tail. In Figure 16 a comparison is made between the experimental distributions of L and the universal distribution used by Bradshaw, Ferriss and Atwell (1967) in the calculation of thin boundary layers. From Figures 16 and 17 it is clear that there is a systematic and dramatic decrease in the mixing length and eddy viscosity as the boundary layer thickness increases in relation to the local radius of the surface.

In recent discussions of energy transport processes in thin boundary layers the mixing length is often associated with a dissipation length on the assumption that the production and dissipation of turbulent kinetic energy are much larger than either diffusion or convection in the wall region, and nearly balance each other. If such an interpretation is accepted for the present case, the reduction in mixing length observed here implies that the rate of dissipation in a thick boundary layer is larger than that in a thin boundary layer. This, coupled with the lower rates of production resulting from the reduced Reynolds stresses, would appear to suggest that the near equilibrium between production and dissipation is no longer maintained in the thick boundary layer, and that increased rate of dissipation must be accompanied by increased rates of convection and diffusion. More detailed turbulence measurements are obviously needed in order to verify these observations.

VII. CONCLUSIONS

Perhaps the most useful purpose served by the present study is the collection of a complete set of experimental data in a hitherto unexplored situation. This data can form the basis for further theoretical studies on a number of aspects of turbulent boundary layer behavior. In view of this, all the experimental results are reproduced in the form of tables in the Appendix.

The major conclusions of this study may be summarized as follows:

1. The turbulent boundary layer on the conical tail of a body of revolution thickens very rapidly. This thickening is accompanied by (a) significant variations in static pressure across the boundary layer such that fluid elements further away from the surface experience less adverse pressure gradients than those nearer the surface; (b) a strong divergence of the mean-flow streamlines in planes normal to the surface, so that the normal velocity component cannot be neglected in comparison with the longitudinal component; and (c) a dramatic decrease in the Reynolds stresses, so that empirical laws established for turbulence behavior in thin boundary layers cannot be used, unmodified, for the prediction of thick boundary layers.

2. The static pressure variation across the boundary layer implies an interaction between the turbulent rotational flow within the boundary layer and the potential flow outside, with the result that neither can be calculated independently of the other.

3. In order to calculate the development of the thick boundary layer, it will be necessary to include not only the direct effects of pressure variation but also the indirect effect of transverse curvature on the turbulence as reflected in the decrease of mixing length and eddy viscosity.

4. The boundary layer calculation is made all the more difficult by the fact that potential flow theory, which ignores the presence of the boundary layer, can no longer be relied upon to predict the pressure field required to calculate the boundary layer development. The prediction of the

flow in the tail region of a body of revolution must therefore be accomplished by an iterative procedure in which potential flow and boundary layer calculations are performed simultaneously. Further discussion of the differential and integral equations of thick axisymmetric boundary layers, and the problems associated with their solution, is given in a recent paper by Patel (1973).

REFERENCES

Bradshaw, P., Ferriss, D.H., and Atwell, N.P., 1967, "Calculation of Boundary Layer Development Using the Turbulent Energy Equation," *J. Fluid Mech.*, *28*, 593.

Cebeci, T., 1970, "Laminar and Turbulent Incompressible Boundary Layers on Slender Bodies of Revolution in Axial Flow," *J. Basic Eng.*, Trans. ASME, Ser. D, *92*, 545.

Chevray, R., 1968, "The Turbulent Wake of a Body of Revolution," *J. Basic Eng.*, Trans. ASME, Ser. D, *90*, 275; Also Ph.D. Thesis, University of Iowa, Iowa City, Iowa, 1967.

Clauser, F.H., 1956, "The Turbulent Boundary Layer," *Advances in Applied Mechanics*, *4*, 1, Academic Press.

Glover, J.R., 1972, "Old Gold Model, Type 4-2H Hot-Wire Anemometer and Type 2 Mean-Product Computer," Iowa Institute of Hydraulic Research, Report No. 136.

Klebanoff, P.S., 1955, "Characteristics of Turbulence in a Boundary Layer with Zero Pressure Gradient," NACA Tech. Report No. 1247.

Laufer, J., 1954, "The Structure of Turbulence in Fully Developed Pipe Flow," NACA Tech. Report No. 1174.

Naudascher, E., 1964, "Effect of Density on Air-Tunnel Measurements," *J. Royal Aeron. Soc.*, *68*, 419.

Patel, V.C., 1965, "Calibration of the Preston Tube and Limitations on Its Use in Pressure Gradients," *J. Fluid Mech.*, *23*, 185.

Patel, V.C., 1972, "A Unified View of the Law of the Wall Using Mixing-Length Theory," Iowa Institute of Hydraulic Research, Report No. 137.

Patel, V.C., 1973, "On the Equations of a Thick Axisymmetric Turbulent Boundary Layer," Iowa Institute of Hydraulic Research, Report No. 143.

Richmond, R.L., 1957, "Experimental Investigation of Thick Axially Symmetric Boundary Layers on Cylinders at Subsonic and Hypersonic Speeds," Ph.D. Thesis, California Institute of Technology, Pasadena, California.

Satija, K.S., 1971, "On the Thick Boundary Layer Near the Tail of a Body of Revolution," Ph.D. Thesis, University of Iowa, Iowa City, Iowa.

Thompson, B.G.J., 1965, "A New Two-Parameter Family of Mean Velocity Profiles for Incompressible Turbulent Boundary Layers on Smooth Walls," British Aero. Res. Council, R & M 3463.

Yasuhara, M., 1959, "Experiments of Axisymmetric Boundary Layers Along a Cylinder in Incompressible Flow," *Trans. Japan Soc. Aerospace Sci.*, *2*, 33.

APPENDIX

TABLES OF EXPERIMENTAL DATA

Station	X/L	r_o (ft)	δ (ft)	Q_δ/U_{ref}	C_{pw}	$C_{p\delta}$	$\bar{\delta}_1$ (ft)	$\bar{\delta}_2$ (ft)	$\bar{H}$	δ_1 (ft)	δ_2 (ft)	H	δ_1^* (ft)	δ_2^* (ft)	H^*	Preston Tube	Clauser Plot	Thompson
																← $C_f \times 10^3$ →		
1	0.662	0.387	0.059	1.030	-0.0461	-0.040 -0.035* -0.030**	0.0100 (0.0096)	0.0071 (0.0068)	1.4009 (1.4055)	0.0103 (0.0099)	0.0074 (0.0071)	1.4099 (1.3978)	0.0110	0.0078	1.3964	3.424	3.40	3.70
2	0.800	0.314	0.082	1.0085	-0.0132	0.0082 0.011* 0.009**	0.0142 (0.0142)	0.0101 (0.0098)	1.4111 (1.445)	0.0152 (0.0152)	0.0108 (0.0106)	1.3978 (1.4287)	0.0151	0.0108	1.4009	3.030	3.00	3.30
3	0.850	0.270	0.103	0.996	0.0395	0.0505 0.034* 0.051**	0.0167 (0.0184)	0.0117 (0.0124)	1.4299 (1.4878)	0.0183 (0.0202)	0.0130 (0.0138)	1.4093 (1.4623)	0.0179	0.0128	1.4006	2.726	2.90	2.90
4	0.900	0.210	0.130	0.977	0.0943	0.0952 0.066* 0.089**	0.0238	0.0156	1.5262	0.0273	0.0184	1.4852	0.0256	0.0176	1.4585	2.185	2.18	2.45
5	0.930	0.157	0.171	0.965	0.1570	0.102 0.095* 0.116**	0.0386	0.0232	1.6630	0.0486	0.0307	1.5837	0.0404	0.0270	1.5005	1.324	1.45	1.80
6	0.960	0.090	0.230	0.963	0.2130	0.109 0.101* 0.130**	0.0658	0.0338	1.9491	0.1067	0.0617	1.7281	0.0713	0.0473	1.5098	0.544	0.60	0.99
7	0.990	0.022	0.286	0.967	0.2310	0.103 0.091* 0.114**	0.0971	0.0436	2.2256	0.3776	0.2169	1.7412	0.1137	0.0843	1.3495		0.35	0.56

Note: ** implied by Q_δ measured by single wire probe and total pressure

* implied by Q_δ measured by single wire probe and Bernoulli equation assumed to hold along $y = \delta$

() based on Pitot Static

Table 1. Pressure Variation at $y = \delta$ and $y = 0$, and Integral Parameters

y, ft.	C_P	C_p	Q/Q_δ ***	Q/Q_δ **	Q/Q_δ *	U/Q_δ *	V/Q_δ *	$\sqrt{\overline{u^2}}/Q_\delta$ *	$\sqrt{\overline{v^2}}/Q_\delta$ *	$\sqrt{\overline{w^2}}/Q_\delta$ *	$-20\ \overline{uv}/Q_\delta^2$ *
0.003	0.377		0.586	0.645							
0.005	0.391	-0.037	0.634								
0.008				0.682							
0.010	0.498	-0.040	0.711		0.686	0.686	0.001	0.0774	0.0465	0.0455	0.0320
0.012					0.710	0.710	0.009	0.0756	0.0454	0.0521	0.0300
0.015	0.577	-0.040	0.761		0.743	0.743	0.007	0.0731	0.0445	0.0529	0.0294
0.018				0.783							
0.020	0.643	-0.040	0.801		0.789	0.789	0.006	0.0690	0.0428	0.0500	0.0270
0.023				0.822							
0.025	0.715	-0.040	0.842		0.830	0.830	0.007	0.0647	0.0397	0.0482	0.0240
0.038				0.854							
0.030	0.772	-0.037	0.866		0.861	0.861	0.005	0.0595	0.0369	0.0452	0.0208
0.033				0.887							
0.035	0.830	-0.037	0.902		0.891	0.891	0.004	0.0542	0.0344	0.0414	0.0170
0.038				0.911							
0.040	0.891	-0.035	0.932		0.922	0.922	0.012	0.0495	0.0313	0.0357	0.0128
0.043				0.943							
0.045	0.941	-0.035	0.958		0.955	0.955	0.018	0.0422	0.0270	0.0312	0.0098
0.050	0.983	-0.035	0.978		0.978	0.978	0.021	0.0330	0.0228	0.0254	0.0060
0.053				0.989							
0.055	0.017	-0.033	0.993		0.992	0.992	0.016	0.0254	0.0187	0.0195	0.0028
0.060	1.036	-0.033	1.002		1.002	1.002	0.020	0.0170	0.0144	0.0138	0.0016
0.063				1.007							
0.065	1.040	-0.031	1.003		1.007	1.006	0.026	0.0109	0.0106	0.0100	0.0004
0.070	1.045	-0.031	1.005		1.014	1.003	0.028	0.0073	0.0082	0.0067	0.0002
0.073				1.011							
0.075	1.047	-0.029	1.005		1.018	1.007	0.025	0.0054	0.0058	0.0057	0.0000
0.080					1.011	1.010	0.022	0.0037	0.0046	0.0052	0.0000
0.090					1.009	1.008	0.030	0.0034	0.0035	0.0039	0.0002
0.093				1.012	0.998	0.998	0.034	0.0025	0.0032	0.0045	0.0000

* Cross Wire Probe
** Single Wire Probe
*** Pitot-Static

Table 2(a). Profiles of Pressure Distribution, Mean Velocities and Reynolds Stresses at X/L = 0.662

y, ft.	C_P	C_p	Q/Q_δ ***	Q/Q_δ **	Q/Q_δ *	U/Q_δ *	V/Q_δ *	$\sqrt{\overline{u^2}}/Q_\delta$ *	$\sqrt{\overline{v^2}}/Q_\delta$ *	$\sqrt{\overline{w^2}}/Q_\delta$ *	$-20\ \overline{uv}/Q_\delta^2$ *
0.003	0.272										
0.004	0.294	-0.009									
0.005				0.501							
0.008				0.621							
0.010	0.423	-0.004	0.645	0.641							
0.014					0.677	0.677	0.020	0.0754	0.0433	0.0535	0.0294
0.015	0.493	-0.002	0.694	0.688							
0.017					0.687	0.687	0.018	0.0743	0.0436	0.0533	0.0290
0.020	0.556	-0.002	0.738	0.730	0.712	0.712	0.019	0.0727	0.0421	0.0524	0.0278
0.025	0.614	-0.002	0.774	0.754	0.751	0.750	0.019	0.0692	0.0407	0.0514	0.0254
0.030	0.658	-0.002	0.801	0.781	0.786	0.785	0.028	0.0664	0.0370	0.0502	0.0216
0.035	0.712	-0.000	0.832	0.823	0.820	0.819	0.032	0.0634	0.0369	0.0490	0.0202
0.040	0.759	0.000	0.859	0.849	0.848	0.847	0.033	0.0605	0.0367	0.0472	0.0190
0.045	0.805	0.004	0.883	0.871	0.878	0.877	0.037	0.0582	0.0350	0.0443	0.0164
0.050	0.848	0.007	0.905	0.890	0.900	0.899	0.043	0.0545	0.0330	0.0419	0.0152
0.055					0.923	0.922	0.047	0.0504	0.0307	0.0402	0.0122
0.060	0.928	0.009	0.945	0.933	0.944	0.942	0.056	0.0472	0.0281	0.0370	0.0100
0.065					0.951	0.949	0.055	0.0418	0.0248	0.0329	0.0078
0.070	0.992	0.011	0.976	0.965	0.967	0.965	0.061	0.0372	0.0224	0.0284	0.0054
0.080	1.037	0.013	0.998	0.998	0.997	0.994	0.071	0.0253	0.0173	0.0188	0.0020
0.090	1.058	0.015	1.006	1.008	1.012	1.009	0.078	0.0131	0.0118	0.0125	0.0004
0.100	1.060	0.018	1.006	1.006	1.015	1.012	0.082	0.0067	0.0073	0.0068	0.0000
0.110	1.060	0.018	1.006								
0.120	1.060	0.020	1.005	1.008	1.015	1.010	0.093	0.0032	0.0038	0.0048	0.0000
0.130		0.022	1.006								
0.140		0.024	1.006	1.004	1.013	1.008	0.098	0.0030	0.0049	0.0045	0.0000

* Cross Wire Probe
** Single Wire Probe
*** Pitot-Static

Table 2(b). Profiles of Pressure Distribution, Mean Velocities and Reynolds Stresses at X/L = 0.80

y, ft.	C_P	C_p	Q/Q_δ ***	Q/Q_δ **	Q/Q_δ *	U/Q_δ *	V/Q_δ *	$\sqrt{u^2}/Q_\delta$ *	$\sqrt{v^2}/Q_\delta$ *	$\sqrt{w^2}/Q_\delta$ *	$-20\ \overline{uv}/Q_\delta^2$ *
0.003	0.263			0.530							
0.004	0.263	0.024	0.486								
0.005				0.554							
0.008					0.604	0.604	-0.004	0.0753	0.0434	0.0515	0.0308
0.010	0.384	0.024	0.596	0.614	0.621	0.621	0.001	0.0732	0.0425	0.0512	0.0294
0.015	0.458	0.024	0.655	0.660	0.670	0.670	0.003	0.0699	0.0416	0.0490	0.0276
0.020	0.500	0.024	0.685	0.699	0.707	0.707	0.005	0.0671	0.0404	0.0473	0.0252
0.025	0.548	0.024	0.719	0.734	0.738	0.738	0.007	0.0644	0.0380	0.0471	0.0222
0.030	0.596	0.024	0.751	0.761	0.771	0.771	0.013	0.0638	0.0380	0.0463	0.0216
0.035	0.649	0.024	0.786	0.785	0.799	0.798	0.017	0.0602	0.0368	0.0455	0.0204
0.040	0.691	0.026	0.810	0.807	0.825	0.825	0.019	0.0580	0.0353	0.0441	0.0178
0.045				0.839	0.844	0.844	0.020	0.0554	0.0339	0.0427	0.0170
0.050	0.776	0.024	0.862	0.882	0.869	0.869	0.018	0.0532	0.0321	0.0410	0.0146
0.055					0.883	0.883	0.025	0.0499	0.0306	0.0383	0.0130
0.060	0.842	0.029	0.896	0.924	0.901	0.901	0.030	0.0464	0.0285	0.0367	0.0110
0.065					0.927	0.926	0.032	0.0439	0.0267	0.0340	0.0090
0.070	0.912	0.029	0.934	0.949	0.944	0.943	0.036	0.0410	0.0245	0.0303	0.0078
0.080	0.967	0.031	0.961	0.975	0.957	0.956	0.047	0.0325	0.0196	0.0237	0.0042
0.090	1.013	0.033	0.983	0.988	0.992	0.991	0.052	0.0222	0.0146	0.0172	0.0014
0.100	1.044	0.035	0.999	0.998	0.999	0.998	0.060	0.0114	0.0099	0.0100	0.0004
0.110	1.055	0.035	1.004								
0.120	1.059	0.037	1.005	1.011	1.004	1.002	0.072	0.0035	0.0040	0.0056	0.0000
0.130	1.061	0.040	1.005								
0.140	1.064	0.042	1.005	1.002	1.000	0.997	0.075	0.0028	0.0038	0.0035	0.0000
0.150	1.064	0.042	1.005								
0.160			1.005		0.994	0.991	0.084	0.0031	0.0030	0.0044	0.0000

* Cross Wire Probe
** Single Wire Probe
*** Pitot-Static

Table 2(c). Profiles of Pressure Distribution, Mean Velocities and Reynolds Stresses at X/L = 0.85

y, ft.	C_P	C_p	Q/Q_δ ***	Q/Q_δ **	Q/Q_δ *	U/Q_δ *	V/Q_δ *	$\sqrt{\overline{u^2}}/Q_\delta$ *	$\sqrt{\overline{v^2}}/Q_\delta$ *	$\sqrt{\overline{w^2}}/Q_\delta$ *	$-20\ \overline{uv}/Q_\delta^2$ *
0.003											
0.004	0.246	0.081	0.412	0.435							
0.005				0.468							
0.010	0.344	0.081	0.522	0.540							
0.012					0.537	0.537	0 015	0.0728	0.0399	0.0467	0.0236
0.015	0.395	0.081	0.570	0.580	0.578	0.578	0.011	0.0705	0.0394	0.0457	0.0226
0.017					0.600	0.600	0.016	0.0686	0.0389	0.0447	0.0224
0.020	0.443	0.079	0.614	0.603	0.628	0.628	0.021	0.0678	0.0382	0.0442	0.0208
0.025	0.487	0.079	0.650	0.620	0.660	0.659	0.024	0.0663	0.0375	0.0442	0.0194
0.030	0.522	0.079	0.677	0.662	0.692	0.691	0.034	0.0646	0.0369	0.0440	0.0184
0.035				0.694	0.720	0.719	0.041	0.0641	0.0361	0.0431	0.0170
0.040	0.594	0.081	0.729	0.706	0.746	0.744	0.049	0.0616	0.0359	0.0423	0.0162
0.045				0.723	0.771	0.769	0.054	0.0600	0.0346	0.0419	0.0150
0.050	0.675	0.083	0.783	0.752	0.792	0.789	0.062	0.0594	0.0338	0.0413	0.0142
0.055					0.816	0.813	0.071	0.0579	0.0319	0.0398	0.0130
0.060	0.739	0.086	0.823	0.784	0.834	0.830	0.075	0.0557	0.0318	0.0387	0.0112
0.070	0.792	0.083	0.857	0.853	0.871	0.866	0.093	0.0528	0.0296	0.0365	0.0094
0.080	0.853	0.083	0.893	0.887	0.897	0.891	0.103	0.0472	0.0268	0.0331	0.0072
0.090	0.908	0.083	0.924	0.926	0.928	0.921	0.115	0.0427	0.0236	0.0285	0.0050
0.100	0.961	0.083	0.954	0.951	0.957	0.949	0.124	0.0371	0.0195	0.0240	0.0026
0.110	1.002	0.083	0.976	0.972							
0.120	1.033	0.083	0.992	0.990	0.993	0.981	0.150	0.0203	0.0124	0.0136	0.0004
0.130	1.048	0.083	1.000								
0.140	1.055	0.081	1.005	1.010	1.007	0.994	0.165	0.0067	0.0068	0.0070	0.0000
0.150	1.055	0.079	1.006								
0.160	1.055	0.079	1.006	1.016	1.010	0.994	0.176	0.0039	0.0041	0.0041	0.0000
0.170	1.053	0.077	1.006								
0.180	1.053	0.077	1.006	1.018							
0.190	1.053	0.077	1.006								
0.200			1.006	1.021	1.007	0.988	0.195	0.0022	0.0057	0.0041	0.0000

* Cross Wire Probe
** Single Wire Probe
*** Pitot-Static

Table 2(d). Profiles of Pressure Distribution, Mean Velocities and Reynolds Stresses at X/L = 0.90

y, ft.	C_P	C_p	Q/Q_δ ***	Q/Q_δ **	Q/Q_δ *	U/Q_δ *	V/Q_δ *	$\sqrt{\overline{u^2}}/Q_\delta$ *	$\sqrt{\overline{v^2}}/Q_\delta$ *	$\sqrt{\overline{w^2}}/Q_\delta$ *	$-20\ \overline{uv}/Q_\delta^2$ *
0.003											
0.004	0.243	0.154	0.307								
0.008											
0.010	0.300	0.151	0.395	0.376							
0.013					0.435	0.435	0.012	0.0753	0.0417	0.0465	0.0242
0.015				0.431	0.451	0.451	0.020	0.0727	0.0403	0.0468	0.0230
0.020	0.375	0.151	0.483	0.486	0.487	0.486	0.031	0.0706	0.0387	0.0454	0.0204
0.025				0.513	0.524	0.523	0.041	0.0692	0.0378	0.0457	0.0180
0.030	0 442	0.151	0.552	0.556	0.555	0.552	0.055	0.0672	0.0369	0.0454	0.0166
0.035				0.581	0.584	0.580	0.067	0.0651	0.0367	0.0447	0.0152
0.040	0.507	0.149	0.610	0.611	0.612	0.608	0.074	0.0646	0.0357	0.0446	0.0142
0.045					0.635	0.629	0.082	0.0638	0.0353	0.0442	0.0126
0.050	0.563	0.149	0.658	0.659	0.663	0.656	0.092	0.0636	0.0348	0.0436	0.0120
0.060	0.616	0.147	0.700	0.702	0.708	0.700	0.110	0.0620	0.0342	0.0429	0.0102
0.070	0.671	0.143	0.743	0.735	0.747	0.735	0.131	0.0595	0.0332	0.0419	0.0086
0.080	0.726	0.138	0.783	0.766	0.785	0.771	0.150	0.0579	0.0312	0.0404	0.0072
0.090	0.772	0.134	0.816	0.808	0.819	0.802	0.165	0.0553	0.0302	0.0388	0.0056
0.100	0.822	0.129	0.850	0.839	0.851	0.833	0.177	0.0515	0.0277	0.0363	0.0042
0.110	0.873	0.125	0.884								
0.120	0.914	0.121	0.910	0.902	0.913	0.887	0.216	0.0447	0.0255	0.0295	0.0020
0.130	0.956	0.114	0.938								
0.140	0.991	0.110	0.959	0.954	0.963	0.931	0.245	0.0325	0.0171	0.0206	0.0004
0.160	1.046	0.101	0.994	0.987	0.996	0.959	0.267	0.0162	0.0130	0.0101	0.0004
0.180	1.064	0.092	1.006	1.001	1.004	0.964	0.279	0.0053	0.0051	0.0049	0.0000
0.200	1.068	0.088	1.010	1.001	1.000	0.958	0.288	0.0036	0.0041	0.0039	0.0002
0.220	1.064	0.081	1.011		1.002	0.957	0.298	0.0034	0.0035	0.0038	0.0000
0.240	1.059	0.077	1.011								
0.260	1.053	0.070	1.011		1.007	0.957	0.313	0.0033	0.0047	0.0036	0.0002

* Cross Wire Probe
** Single Wire Probe
*** Pitot-Static

Table 2(e). Profiles of Pressure Distribution, Mean Velocities and Reynolds Stresses at X/L = 0.93

y, ft.	C_P	C_p	Q/Q_δ ***	Q/Q_δ **	Q/Q_δ *	U/Q_δ *	V/Q_δ *	$\sqrt{\overline{u^2}}/Q_\delta$ *	$\sqrt{\overline{v^2}}/Q_\delta$ *	$\sqrt{\overline{w^2}}/Q_\delta$ *	$-20\ \overline{uv}/Q_\delta^2$ *
0.006				0.191							
0.008				0.215							
0.010	0.263	0.219	0.213	0.233							
0.015				0.262							
0.020	0.296	0.217	0.288	0.293							
0.025				0.333	0.356	0.356	0.017	0.0638	0.0345	0.0399	0.0190
0.027					0.367	0.367	0.017	0.0650	0.0354	0.0410	0.0204
0.030	0.336	0.217	0.352	0.376	0.384	0.383	0.026	0.0649	0.0354	0.0430	0.0198
0.035				0.404	0.414	0.412	0.036	0.0656	0.0357	0.0429	0.0180
0.040	0.377	0.215	0.413	0.443	0.448	0.446	0.048	0.0647	0.0354	0.0426	0.0172
0.045				0.465							
0.050	0.421	0.213	0.468	0.493	0.496	0.492	0.065	0.0628	0.0341	0.0420	0.0142
0.055				0.524							
0.060	0.467	0.211	0.521	0.545	0.542	0.536	0.081	0.0611	0.0338	0.0417	0.0140
0.065				0.567							
0.070	0.511	0.206	0.566	0.583	0.588	0.579	0.103	0.0593	0.0330	0.0411	0.0120
0.075				0.604							
0.080	0.550	0.202	0.606	0.630	0.626	0.614	0.118	0.0587	0.0319	0.0403	0.0106
0.090	0.599	0.195	0.653	0.668	0.662	0.648	0.136	0.0566	0.0311	0.0397	0.0098
0.100	0.647	0.193	0.693	0.710	0.695	0.678	0.153	0.0560	0.0298	0.0391	0.0096
0.110	0.686	0.184	0.729	0.749							
0.120	0.728	0.178	0.761	0.778	0.766	0.743	0.184	0.0538	0.0282	0.0356	0.0068
0.130				0.800							
0.140	0.809	0.160	0.828	0.831	0.838	0.812	0.210	0.0491	0.0264	0.0321	0.0042
0.160	0.893	0.151	0.885	0.884	0.902	0.870	0.237	0.0427	0.0215	0.0270	0.0030
0.180	0.965	0.136	0.935	0.935	0.933	0.897	0.256	0.0333	0.0165	0.0194	0.0000
0.200	1.026	0.127	0.974	0.970	0.968	0.926	0.282	0.0200	0.0118	0.0120	0.0004
0.220	1.059	0.118	0.996	0.996	0.996	0.952	0.295	0.0086	0.0080	0.0058	0.0002
0.240	1.061	0.107	1.003	1.004	1.004	0.956	0.304	0.0038	0.0041	0.0043	0.0000
0.260	1.064	0.101	1.008	1.006	1.008	0.957	0.317	0.0025	0.0043	0.0034	0.0000
0.280			1.012								
0.300					1.017	0.964	0.326	0.0049	0.0030	0.0030	0.0000

* Cross Wire Probe
** Single Wire Probe
*** Pitot-Static

Table 2(f). Profiles of Pressure Distribution, Mean Velocities and Reynolds Stresses at X/L = 0.96

y, ft.	C_p	C_p	Q/Q_δ ***	Q/Q_δ **	Q/Q_δ *	U/Q_δ *	V/Q_δ *	$\sqrt{\overline{u^2}}/Q_\delta$ *	$\sqrt{\overline{v^2}}/Q_\delta$ *	$\sqrt{\overline{w^2}}/Q_\delta$ *	$-20\ \overline{uv}/Q_\delta^2$ *
0.005				0.160							
0.007											
0.010	0.268	0.239	0.170	0.182							
0.015				0.198							
0.020	0.274	0.237	0.196	0.215							
0.025				0.233	0.212	0.212	0.012	0.0376	0.0198	0.0218	0.0072
0.027					0.223	0.223	0.013	0.0400	0.0214	0.0231	0.0084
0.030	0.287	0.232	0.239	0.249	0.241	0.240	0.015	0.0434	0.0231	0.0248	0.0098
0.035					0.269	0.269	0.021	0.0482	0.0256	0.0270	0.0118
0.040	0.304	0.228	0.284	0.304	0.288	0.286	0.032	0.0517	0.0271	0.0296	0.0132
0.045					0.309	0.307	0.035	0.0546	0.0291	0.0321	0.0148
0.050	0.322	0.226	0.319	0.355	0.333	0.330	0.045	0.0577	0.0309	0.0333	0.0160
0.060	0.344	0.224	0.357	0.387	0.388	0.383	0.058	0.0619	0.0335	0.0365	0.0182
0.070	0.373	0.219	0.404	0.432	0.436	0.430	0.073	0.0621	0.0335	0.0391	0.0170
0.080	0.401	0.217	0.443	0.473	0.476	0.468	0.087	0.0619	0.0330	0.0394	0.0150
0.090					0.518	0.507	0.104	0.0595	0.0323	0.0392	0.0140
0.100	0.465	0.208	0.523	0.559	0.539	0.526	0.120	0.0586	0.0319	0.0387	0.0134
0.120	0.535	0.197	0.599	0.628	0.611	0.593	0.149	0.0577	0.0307	0.0380	0.0120
0.140	0.601	0.184	0.666	0.693	0.667	0.645	0.170	0.0561	0.0297	0.0371	0.0088
0.160	0.678	0.175	0.731	0.754	0.739	0.716	0.181	0.0542	0.0283	0.0362	0.0086
0.180	0.752	0.164	0.793	0.813	0.806	0.774	0.222	0.0507	0.0266	0.0338	0.0072
0.200	0.818	0.154	0.842	0.876	0.862	0.825	0.249	0.0469	0.0238	0.0298	0.0048
0.220	0.899	0.143	0.899	0.928							
0.240	0.961	0.129	0.942	0.951	0.957	0.912	0.289	0.0323	0.0153	0.0185	0.0006
0.260	1.015	0.123	0.977	0.987							
0.280	1.046	0.112	0.999	0.993	0.999	0.949	0.313	0.0084	0.0064	0.0054	0.0000
0.300	1.050	0.105	1.005	1.002							
0.320	1.050	0.099	1.007	1.001	1.004	0.951	0.321	0.0034	0.0036	0.0038	0.0002
0.340	1.050	0.094	1.011								
0.360	1.050	0.094	1.013		1.007	0.953	0.325	0.0038	0.0035	0.0034	0.0000

* Cross Wire Probe
** Single Wire Probe
*** Pitot-Static

Table 2(g). Profiles of Pressure Distribution, Mean Velocities and Reynolds Stresses at X/L = 0.99

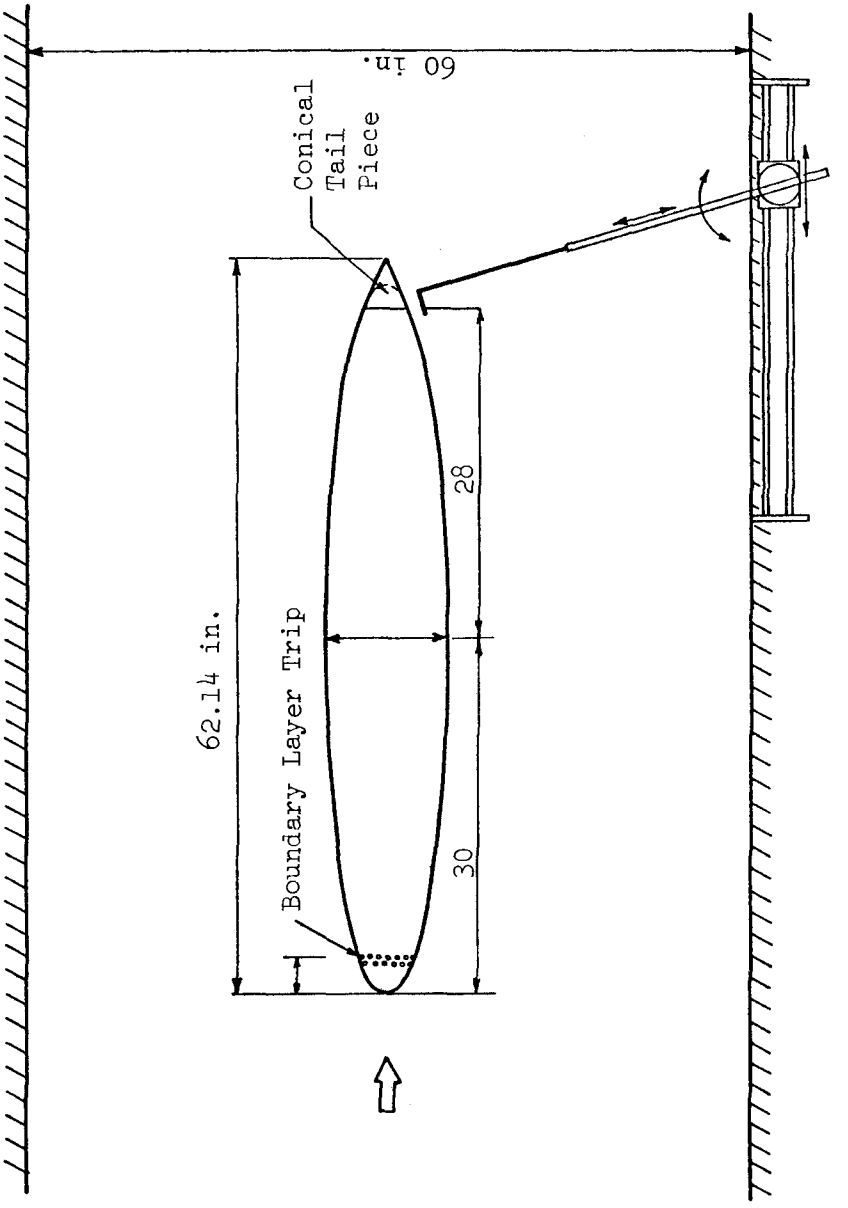

Figure 1. Model and Traversing Mechanism

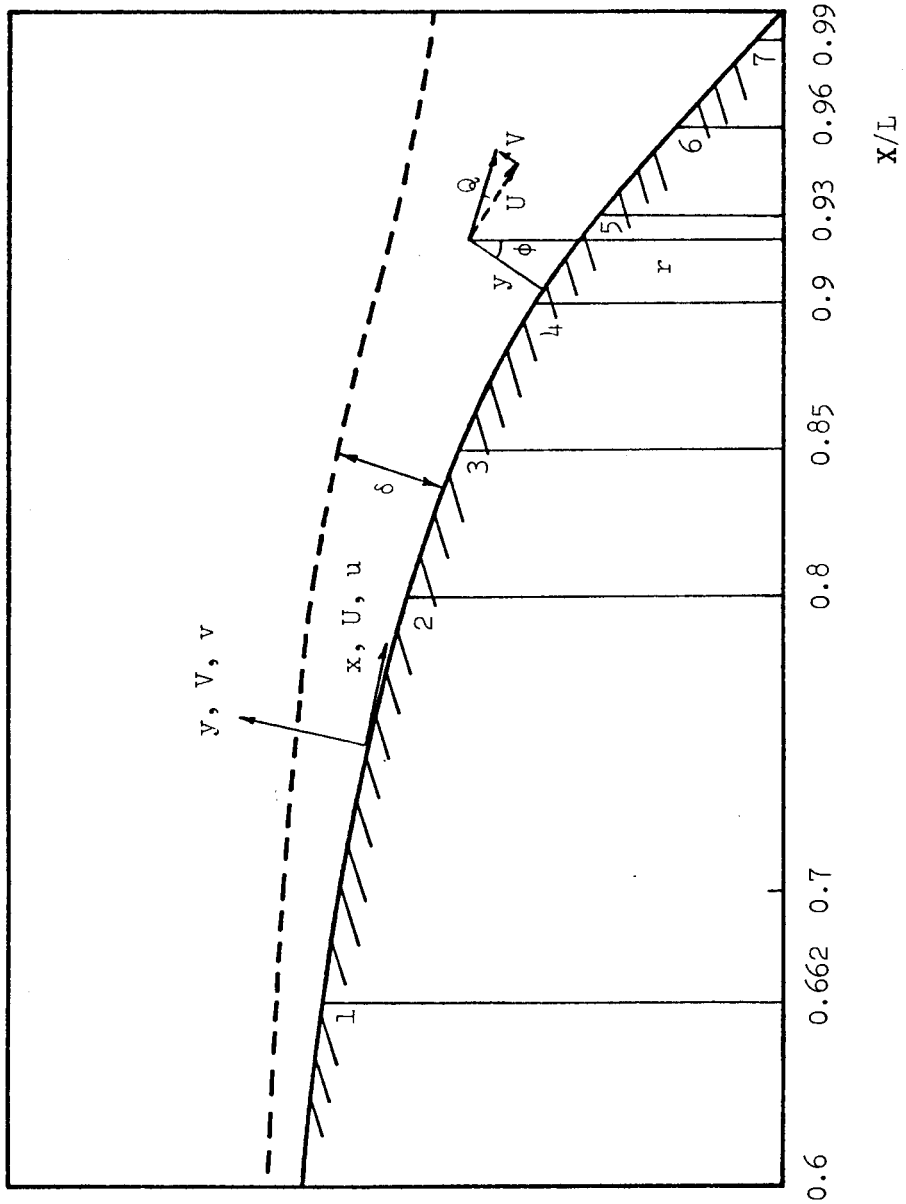

Figure 2. Measuring Stations and Notation

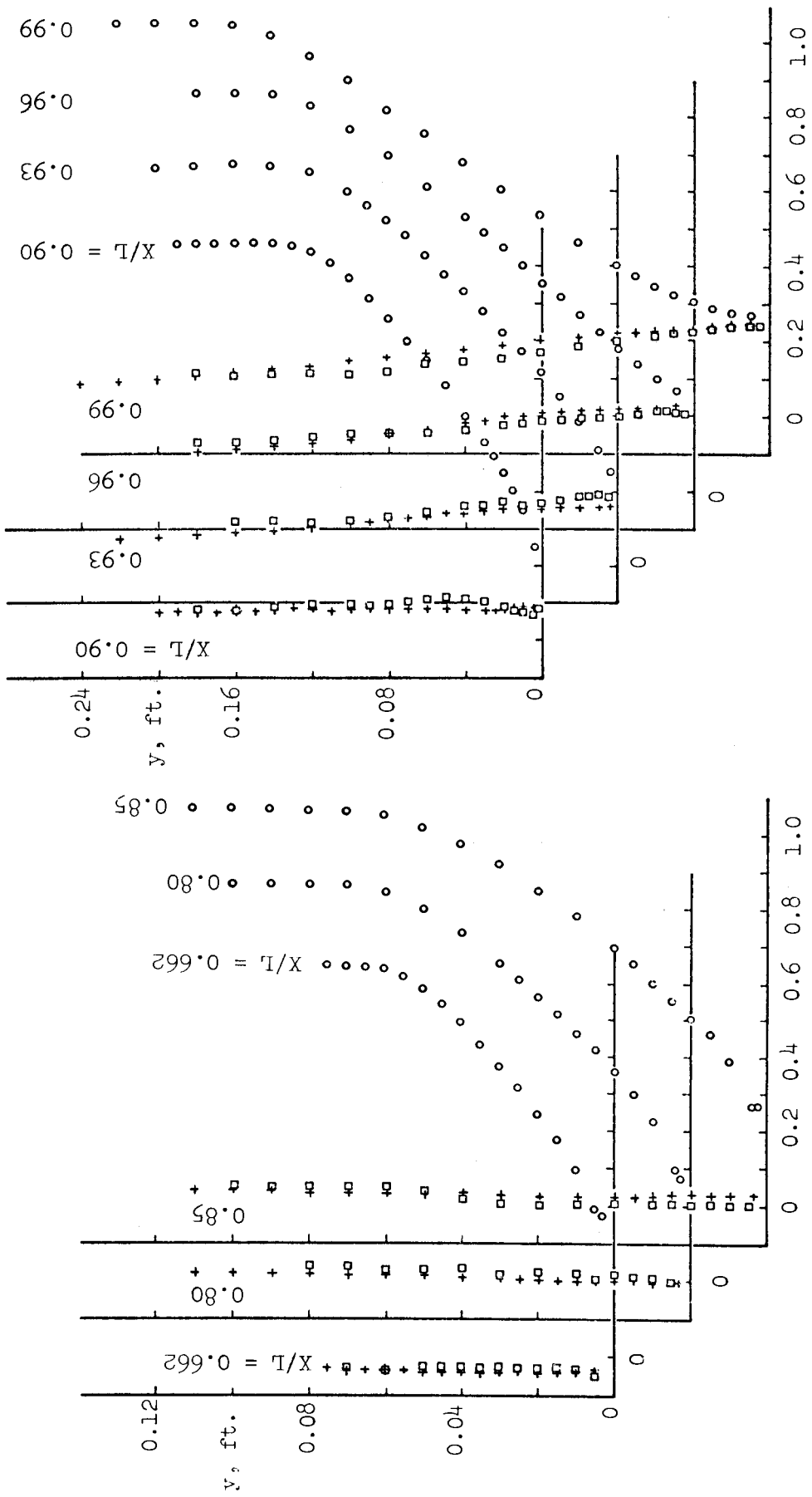

Figure 3. Variation of Total and Static Pressure Coefficients

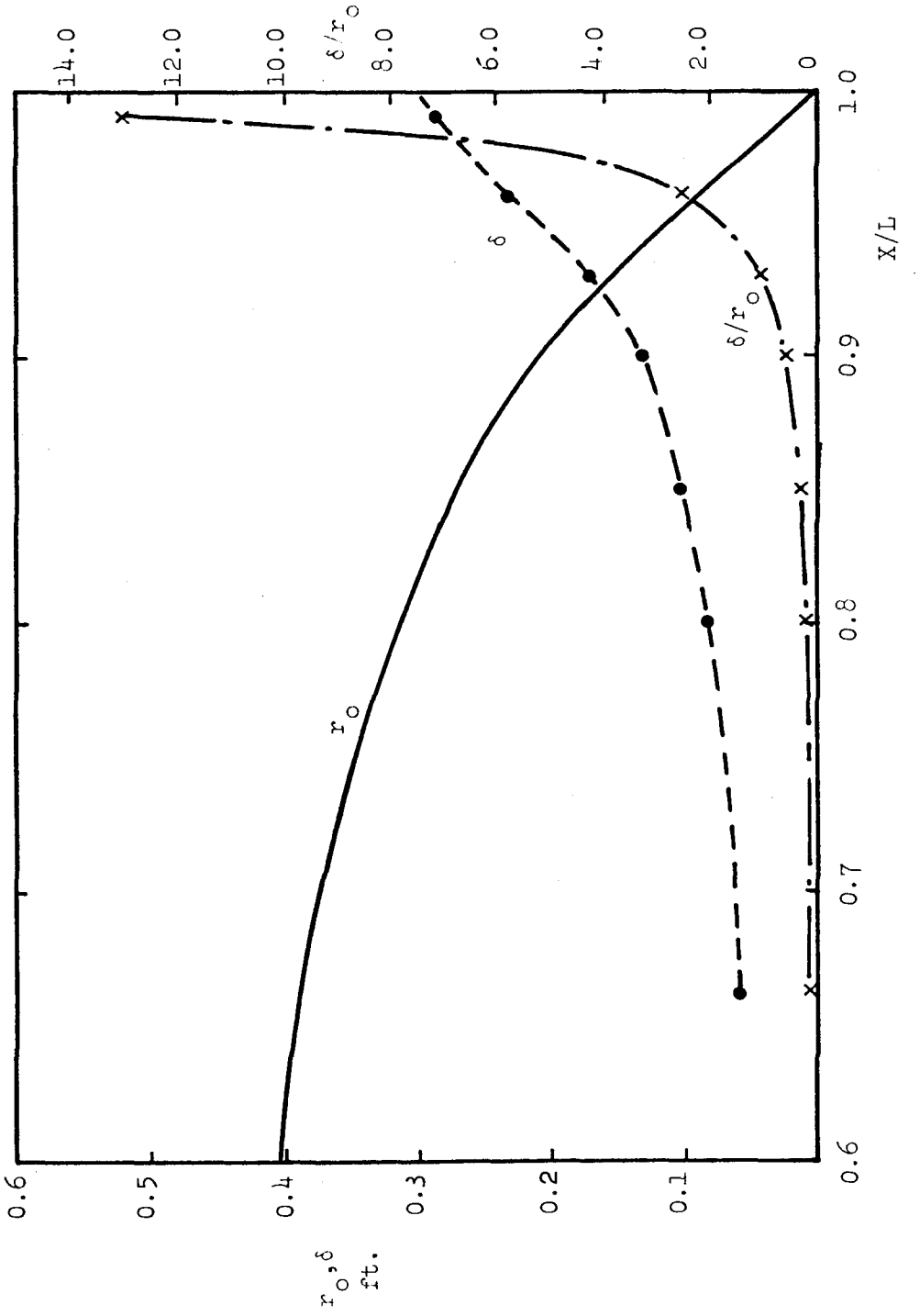

Figure 4. Variation of Boundary Layer Thickness and Local Radius of the Body

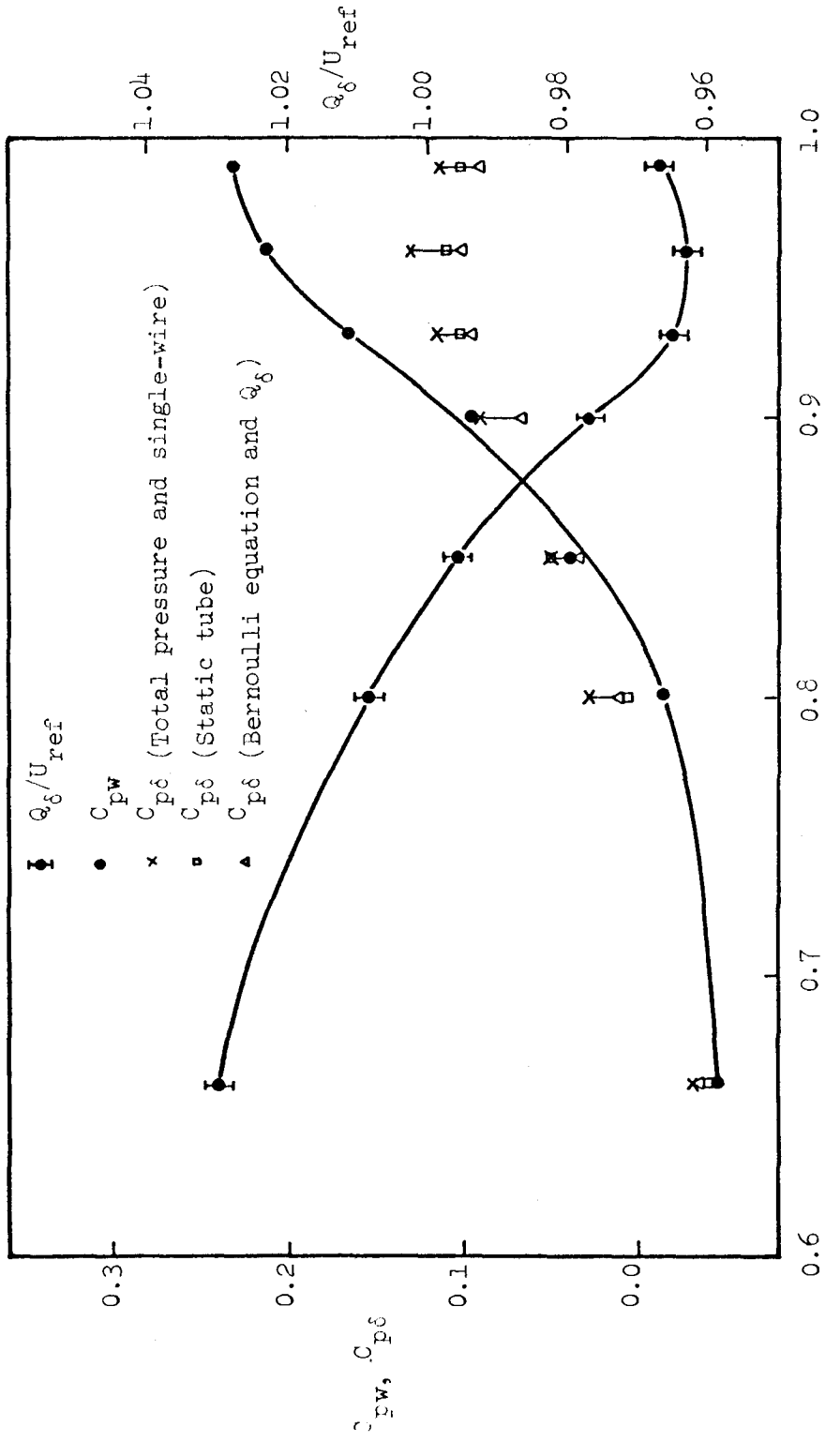

Figure 5. Variation of Wall Static Pressure, and Pressure and Velocity at the Edge of the Boundary Layer

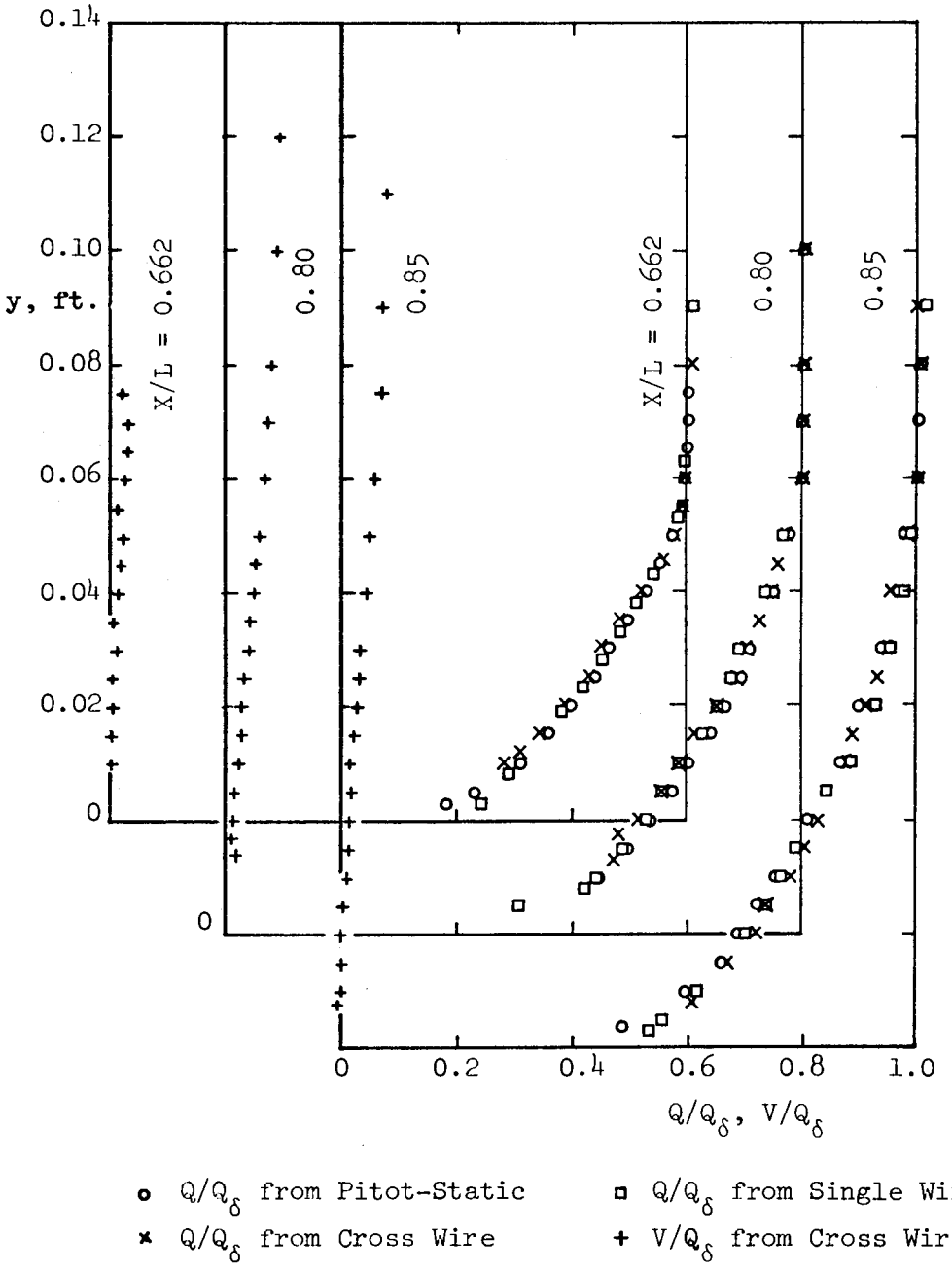

Figure 6-A. Mean Velocity Profiles (X/L = 0.662 ~ 0.85)

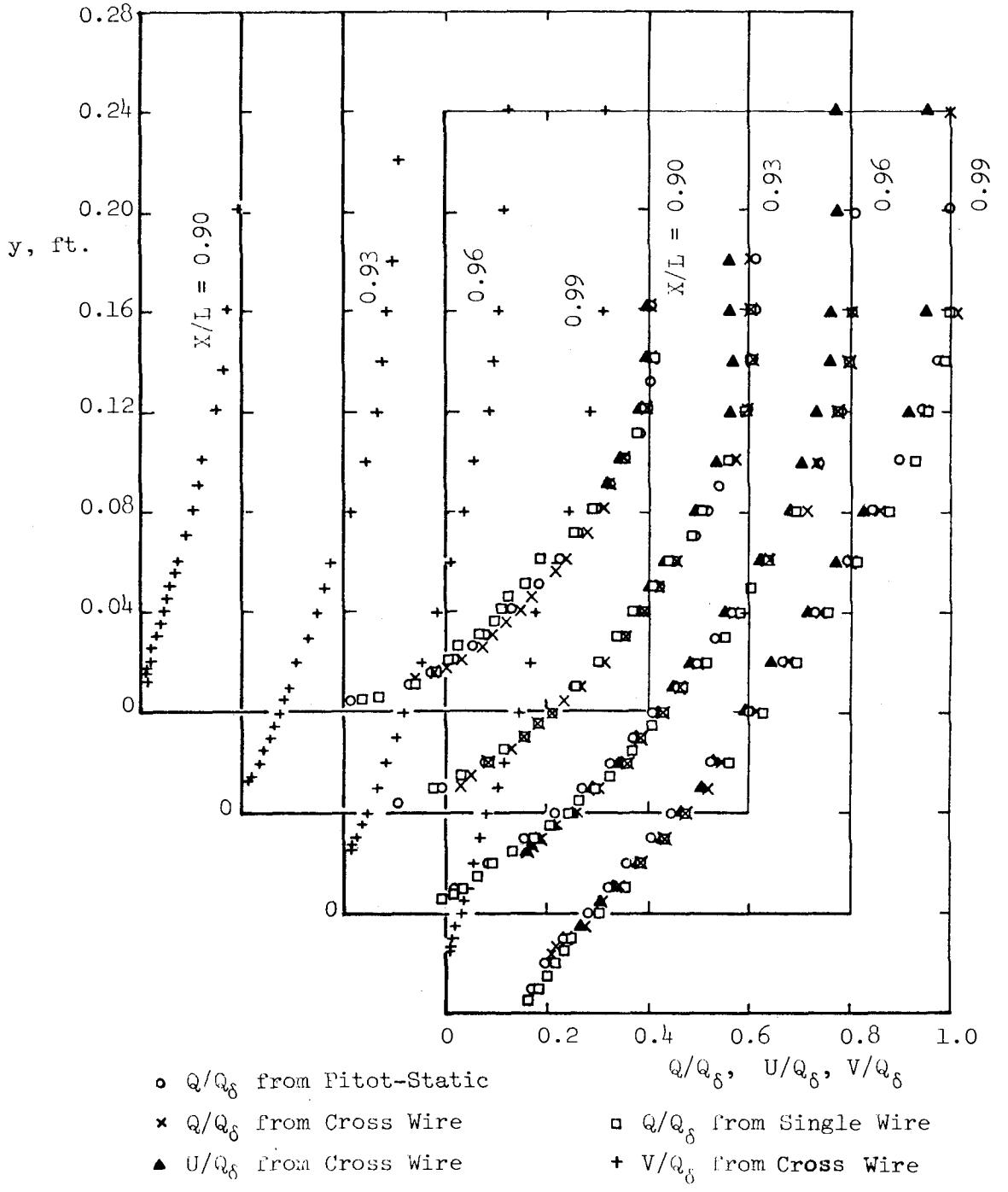

Figure 6-B. Mean Velocity Profiles (X/L = 0.90 ~ 0.99)

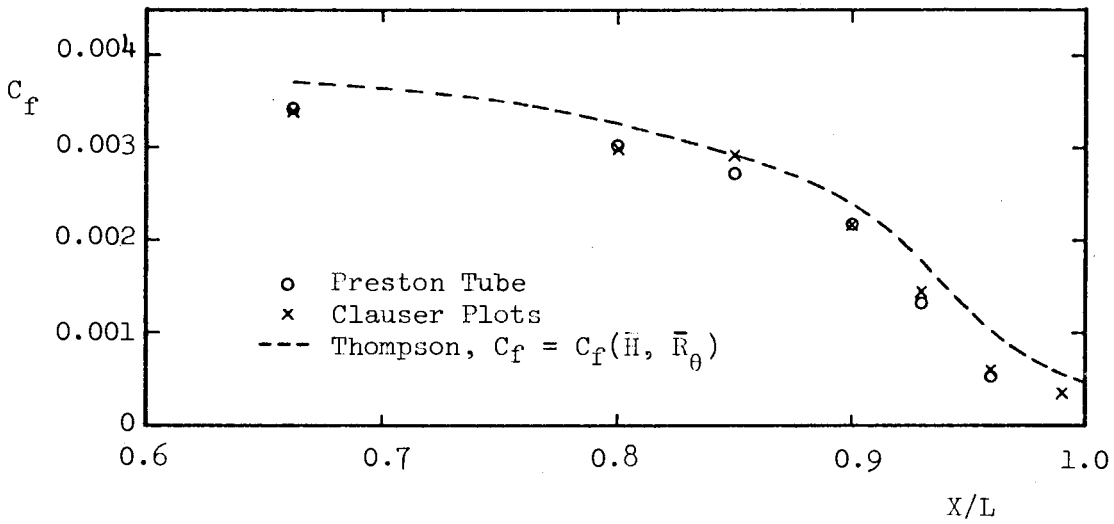

Figure 7. Variation of Skin-Friction Coefficient

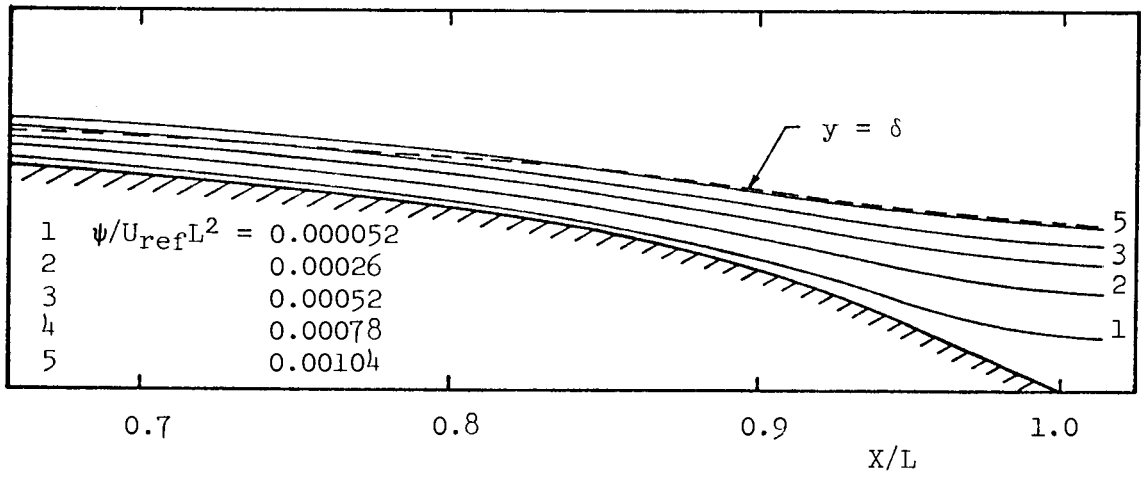

Figure 8. Mean-Flow Streamlines Computed from Velocity Profiles

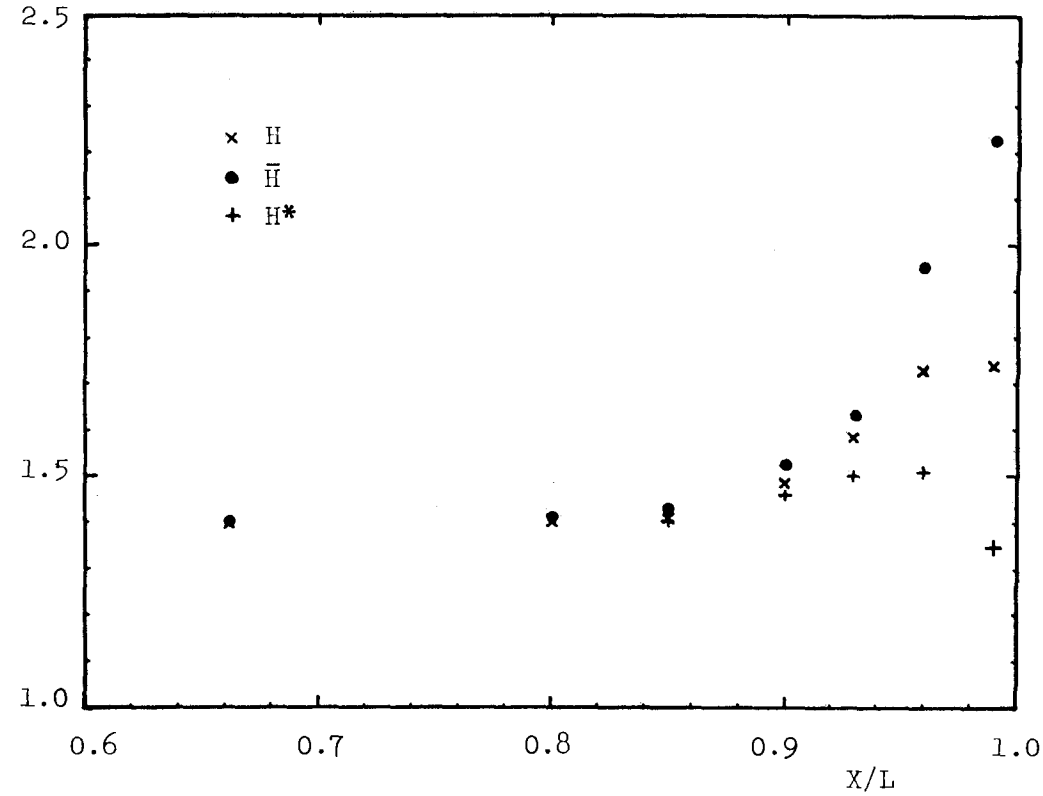

Figure 9. Variation of Shape Factors Using Different Definitions

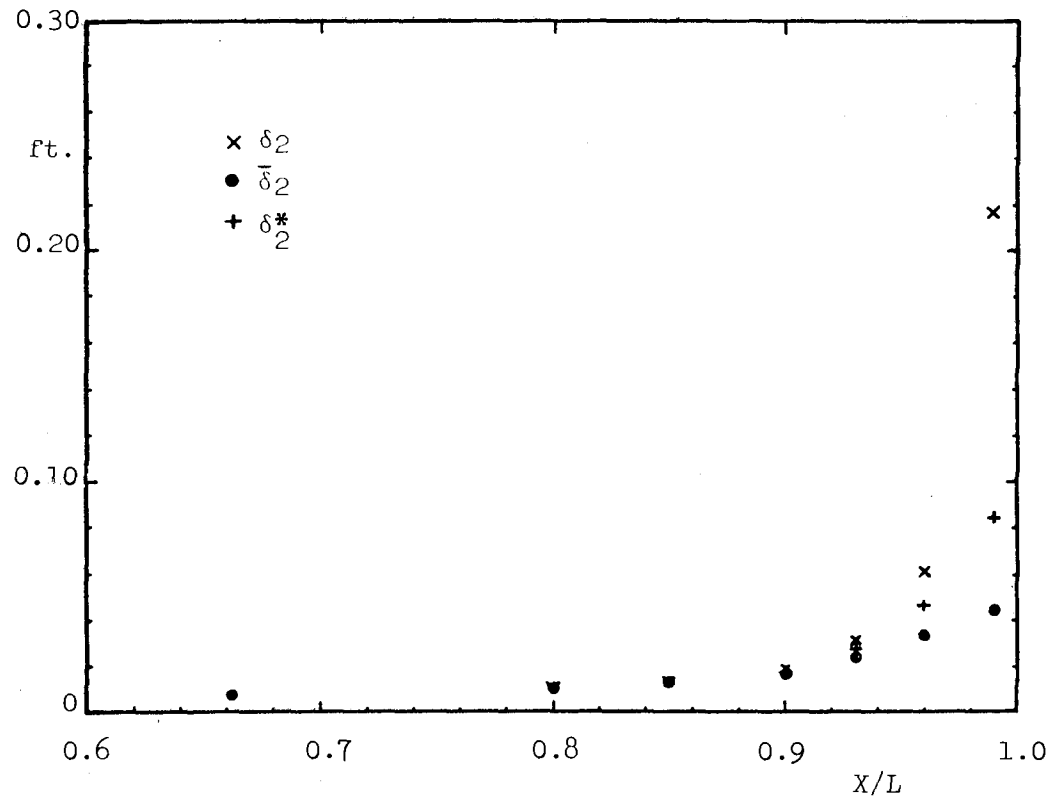

Figure 10. Variation of Momentum Thickness Using Different Definitions

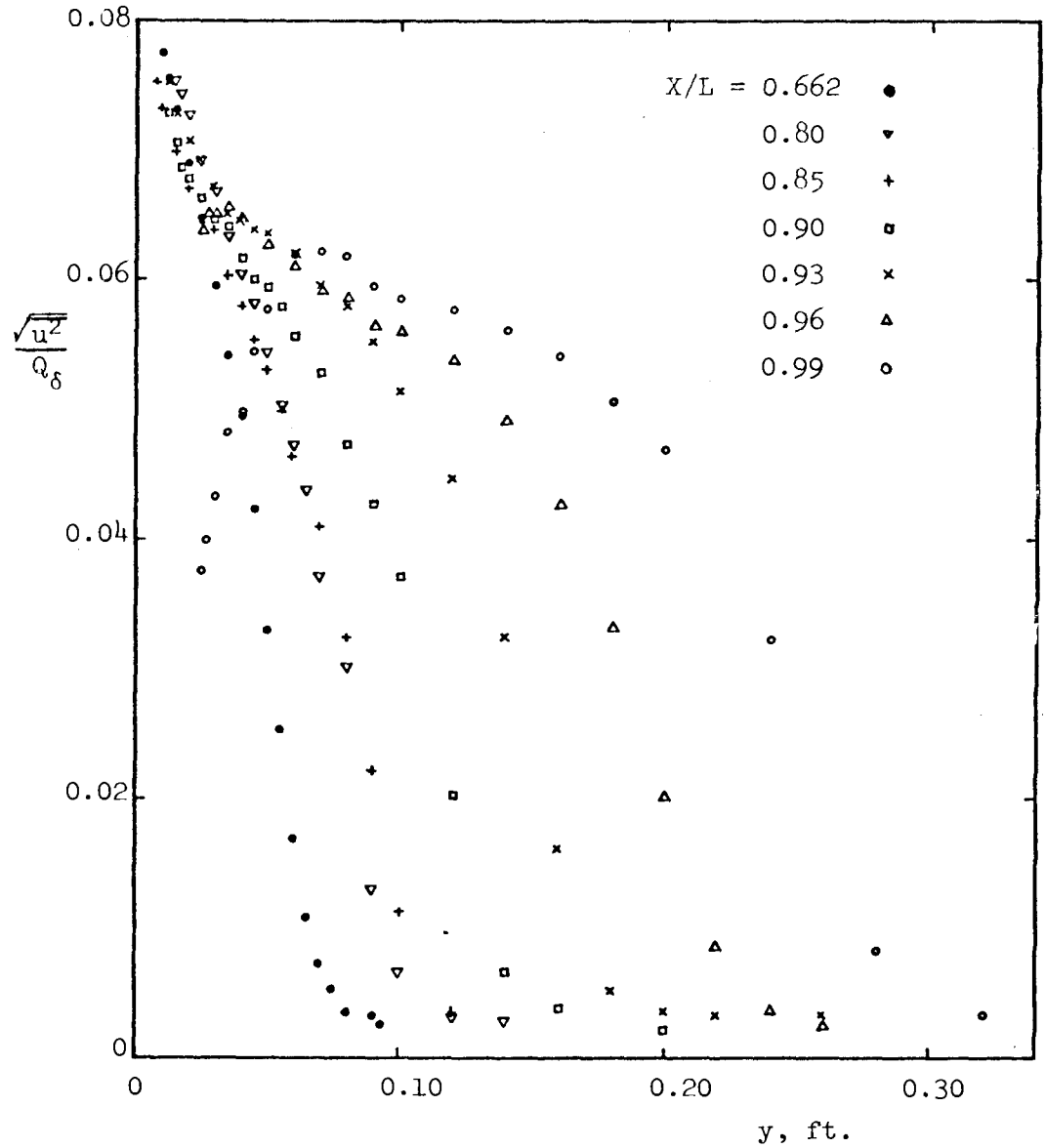

Figure 11. Longitudinal Velocity Fluctuations, $\sqrt{u^2}/Q_\delta$

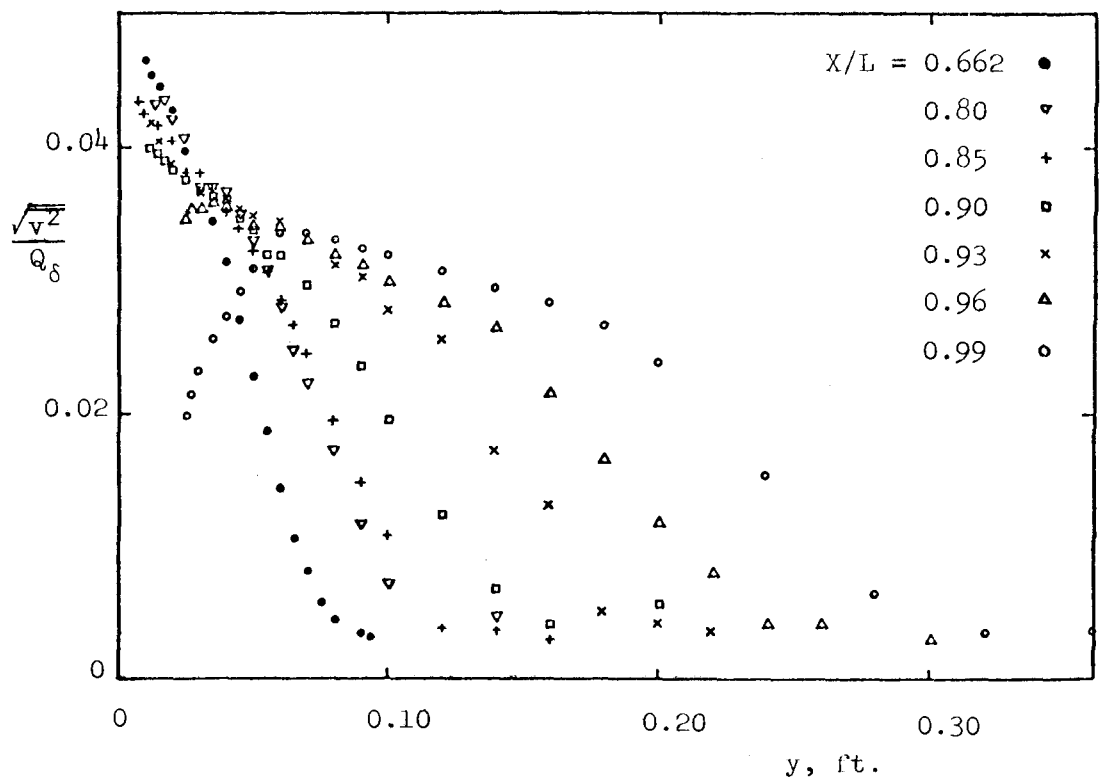

Figure 12. Normal Velocity Fluctuations, $\sqrt{v^2}/Q_\delta$

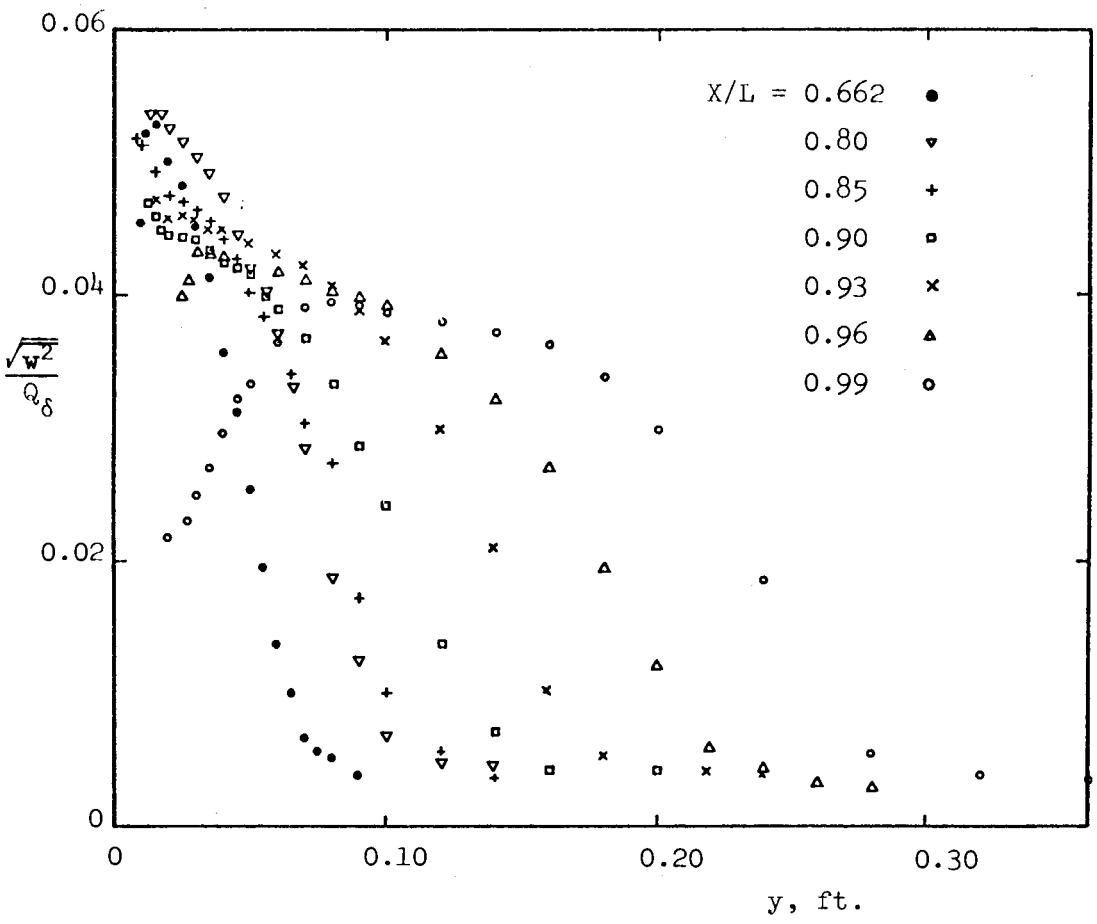

Figure 13. Transverse Velocity Fluctuations, $\sqrt{w^2}/Q_\delta$

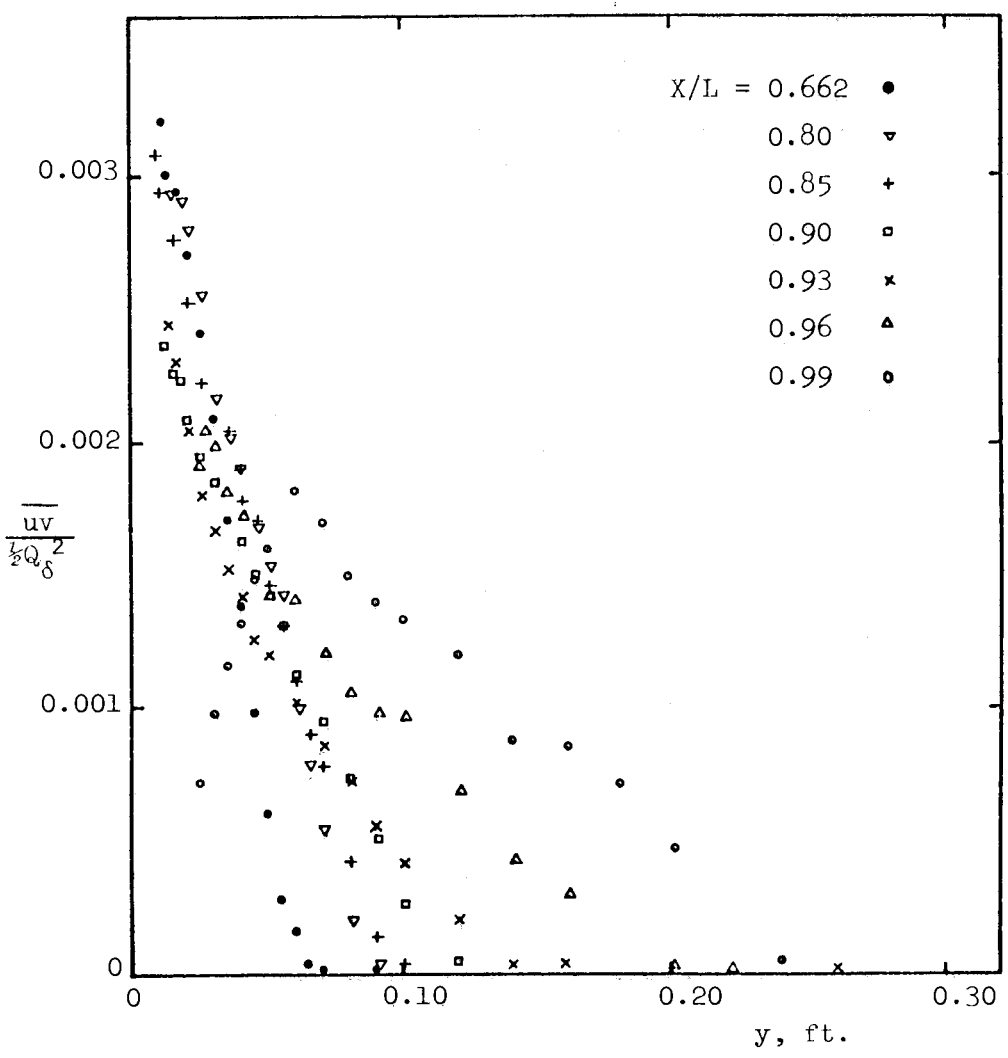

Figure 14. Variation of Reynolds Shear Stress, $\overline{uv}/\frac{1}{2}Q_\delta^2$

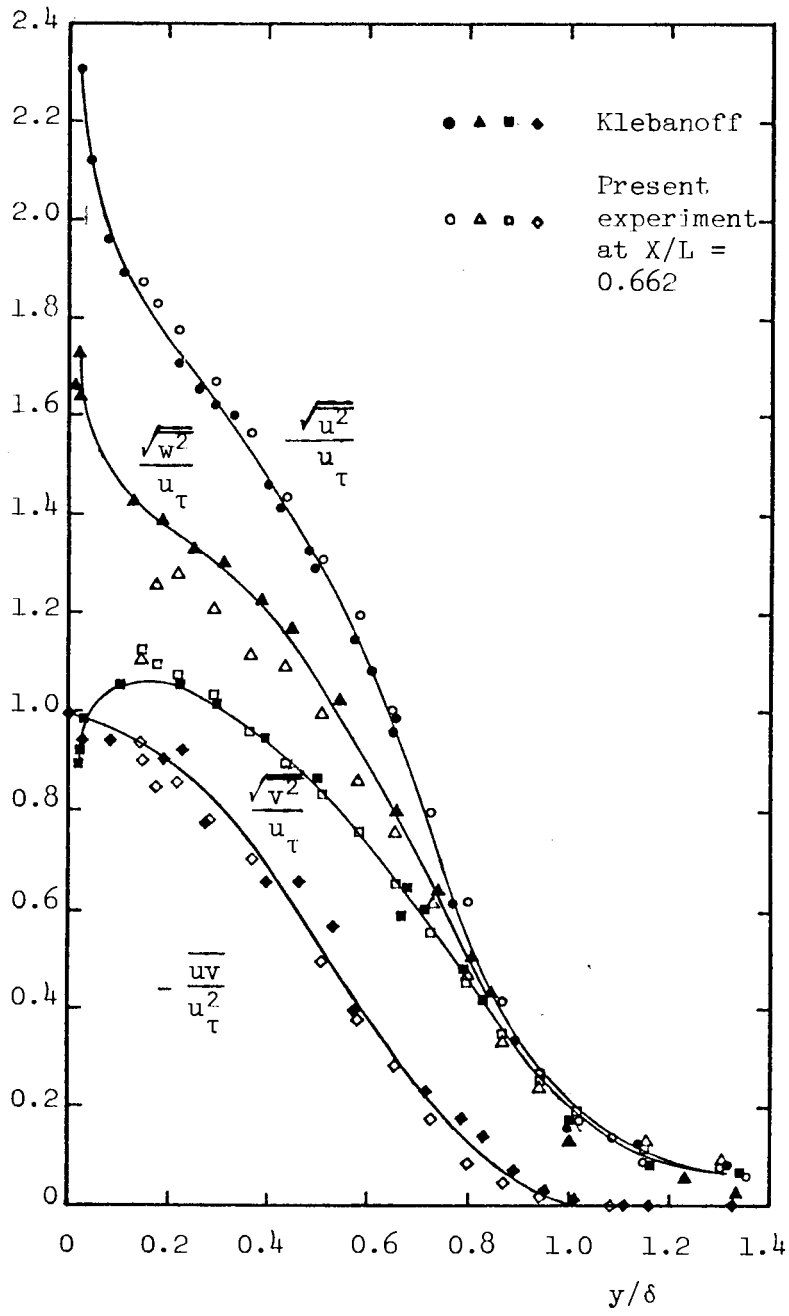

Figure 15. Comparison Between the Turbulence Measurements at X/L = 0.662 and the Data of Klebanoff (1955)

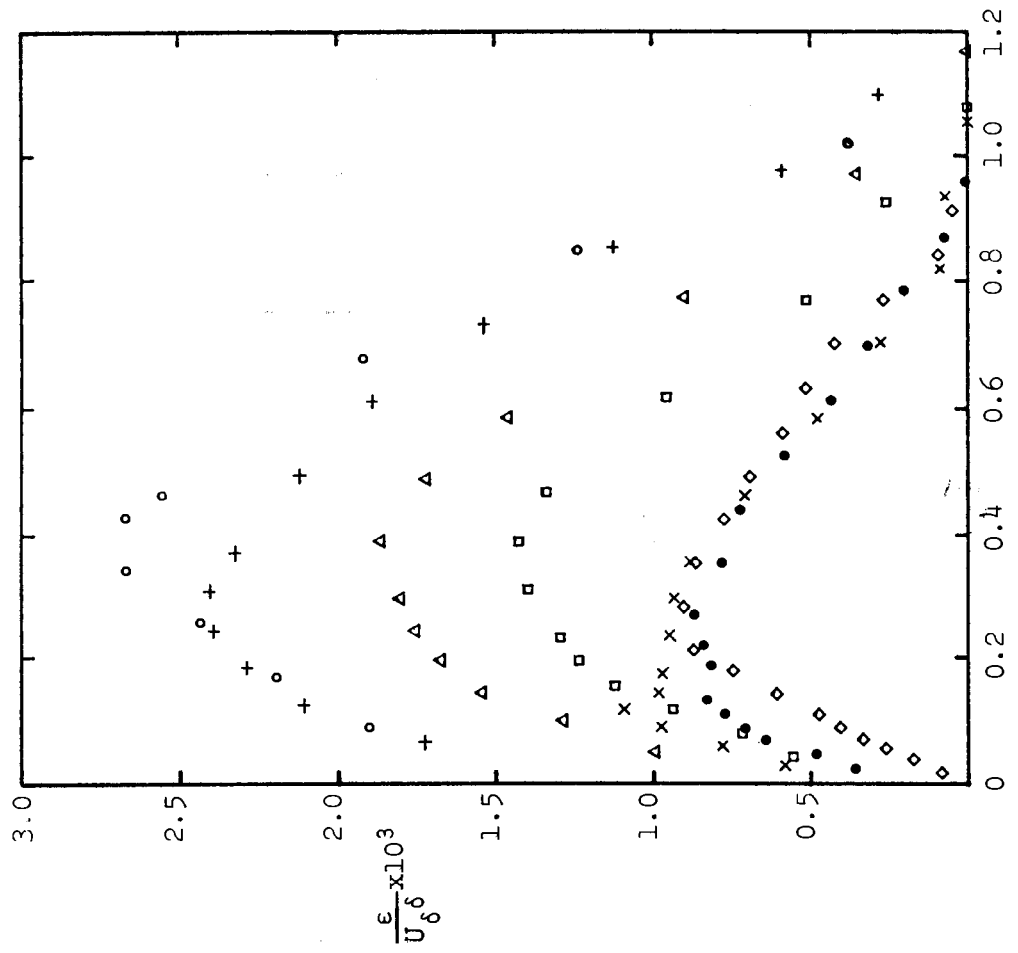

Figure 17. Eddy Viscosity Profiles

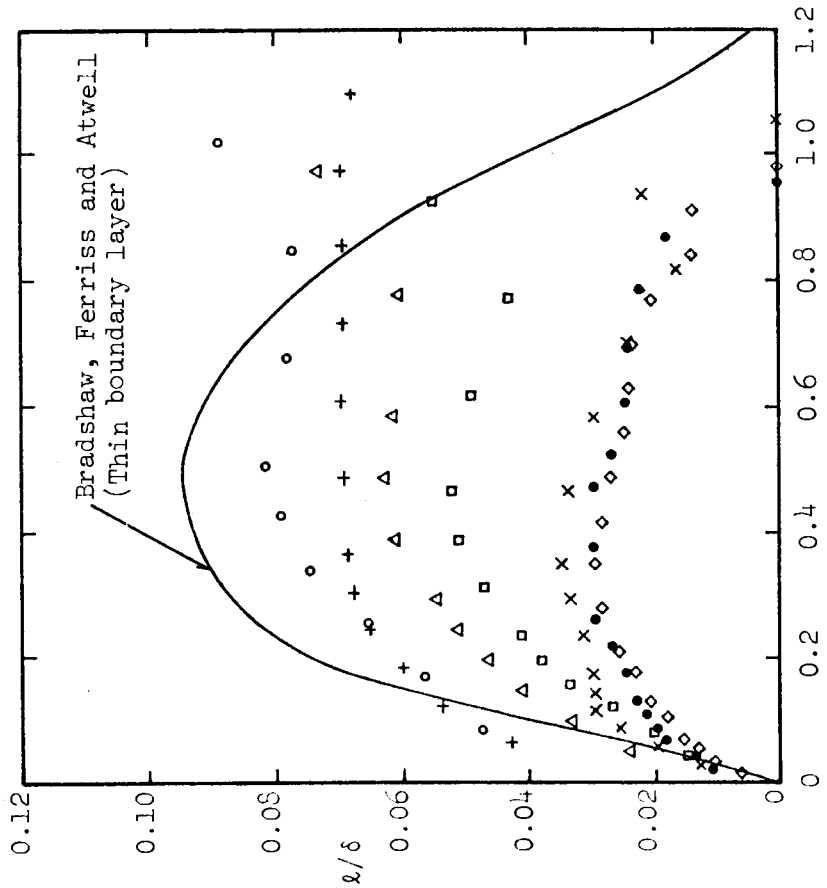

Figure 16. Mixing Length Profiles

NSRDC LIST

March 19, 1973

40 Commander
Naval Ship Research and
Development Center
Bethesday, Maryland 20034
Attn: Code 1505
Code 5614 (39 cys)

1 Officer-in-Charge
Annapolis Laboratory
Naval Ship Research and
Development Center
Annapolis, Maryland 21402
Attn: Code 5642(Library)

6 Commander
Naval Ship Systems Command
Washington, D.C. 20360
Attn: SHIPS 2052 (3 cys)
SHIPS 03412B
SHIPS 0372
SHIPS 0342

12 Director
Defense Documentation Center
5010 Duke Street
Alexandria, Virginia 22314

1 Office of Naval Research
800 N. Quincy Street
Arlington, Virginia 22217
Attn: Mr. R.D. Cooper (Code 438)

1 Office of Naval Research
Branch Office
492 Summer Street
Boston, Mass. 02210

1 Office of Naval Research
Branch Office (493)
536 S. Clark Street
Chicago, Illinois 60605

1 Chief Scientist
Office of Naval Research
Branch Office
1030 E. Green Street
Pasadena, CA 91106

1 Office of Naval Research
Resident Representative
207 West 24th St.
New York, New York 10011

1 Office of Naval Research
Resident Representative
50 Fell Street
San Francisco, Ca 94102

2 Director
Naval Research Laboratory
Washington, D.C. 20390
Attn: Code 2027
Code 2629 (ONRL)

1 Commander
Naval Facilities Engineering
Command (Code 032C)
Washington, D.C. 20390

1 Library of Congress
Science & Technology Division
Washington, D.C. 20540

Commander
Naval Ordnance Systems
Command (ORD 035)
Washington, D.C. 20360

1 Commander
Naval Electronics Laboratory
Center (Library)
San Diego, Ca 92152

8 Commander
Naval Ship Engineering Center
Center Building
Prince Georges Center
Hyattsville, Maryland 20782
Attn: SEC 6034B
SEC 6110
SEC 6114H
SEC 6120
SEC 6136
SEC 6144G
SEC 6140B
SEC 6148

1 Naval Ship Engineering Center
Norfolk Division
Small Craft Engr. Dept.
Norfolk, Virginia 23511
Attn: D. Blount (6660.03)

1 Library (Code 1640)
Naval Oceanographic Office
Washington, D.C. 20390

1 Technical Library
Naval Proving Ground
Dehlgren, Virginia 22448

1 Commander (ADL)
Naval Air Development Center
Warminster, Penna 18974

1 Commanding Officer (L31)
Naval Civil Engineering Laboratory
Port Hueneme, CA 93043

1 Commander
Naval Undersea Center
San Diego, CA 92132
Attn: Dr. A. Fabula (6005)

2 Officer-in-Charge
Naval Undersea Center
Pasadena, CA 91107
Attn: Dr. J. Hoyt (2501)
Library (13111)

1 Director
Naval Research Laboratory
Underwater Sound Reference Division
P.O. Box 8337
Orlando, Flordia 32806

1 Library
Naval Underwater Systems Center
Newport, R.I. 02840

1 Research Center Library
Waterways Experiment Station
Corps of Engineers
P.O. Box 631
Vicksburg, Mississippi 39180

2 National Bureau of Standards
Washington, D.C. 20234
Attn: P. Klebanoff (FM 105)
Fluid Mechanics
Hydraulic Section

1 AFOSR/NAM
1400 Wilson Blvd.
Arlington, Virginia 22209

1 AFFOL/FYS (J. Olsen)
Wright Patterson AFB
Dayton, Ohio 45433

1 Dept. of Transportation
Library TAD-491.1
400 - 7th Street, S.W.
Washington, D.C. 20590

1 Boston Naval Shipyard
Planning Dept. Bldg 39
Technical Library, Code 202.2
Boston, Mass. 02129

1 Charleston Naval Shipyard
Technical Library
Naval Base
Charleston, S.C. 29408

1 Norfolk Naval Shipyard
Technical Library
Portsmouth, Virginia 23709

1 Philadelphia Naval Shipyard
Philadelphia, Penna 19112
Attn: Code 240

1 Portsmouth Naval Shipyard
Technical Library
Portsmouth, N.H. 03801

1 Puget Sound Naval Shipyard
Engineering Library
Bremerton, Wash. 98314

1 Long Beach Naval Shipyard
Technical Library (246L)
Long Beach, CA 90801

1 Hunters Point Naval Shipyard
Technical Library (Code 202.3)
San Francisco, CA 94135

1 Pearl Harbor Naval Shipyard
Code 202.32
Box 400, FPO
San Francisco, CA 96610

1 Mare Island Naval Shipyard
Shipyard Technical Library
Code 202.3
Vallejo, CA 94592

1 Assistant Chief Design Engineer
for Naval Architecture (Code 250)
Mare Island Naval Shipyard
Vallejo, CA 94592

3 U.S. Naval Academy
Annapolis, Maryland 21402
Attn: Technical Library
Dr. Bruce Johnson
Prof. P. Van Mater, Jr.

3 Naval Postgraduate School
Monterey, CA 93940
Attn: Library, Code 2124
Dr. T. Sarpkaya
Prof. J. Miller

1 Capt. L.S. McCready, USMS
Director, National Maritime
Research Center
U.S. Merchant Marine Academyy
Kings Point, L.I., New York 11204
Attn: Academy Library

1 U.S. Merchant Marine Academy
Kings Point, L.I., New York 11204
Attn: Academy Library

1 Library
The Pennsylvania State University
Ordnance Research Laboratory
P.O. Box 30
State College, Penna 16801

1 Bolt, Beranek & Newman
1501 Wilson Blvd.
Arlington, Virginia 22209
Attn: Dr. F. Jackson

1 Bolt, Beranek & Newman
50 Moulton Street
Cambridge, Mass. 02138
Attn: Library

1 Bethlehem Steel Corporation
Center Technical Division
Sparrows Point Yard
Sparrows Point, Maryland 21219

1 Bethlehem Steel Corporation
25 Broadway
New York, New York 10004
Attn: Library (Shipbuilding)

Cambridge Acoustical Associates, Inc.
1033 Mass Avenue
Cambridge, Mass. 02138
Attn: Dr. M. Junger

1 Cornell Aeronautical Laboratory
Aerodynamics Research Dept.
P.O. Box 235
Buffalo, New York 14221
Attn: Dr. A. Ritter

1 Eastern Research Group
P.O. Box 222
Church Street Station
New York, New York 10008

1 Esso International
Design Division, Tanker Dept.
15 West 51st Street
New York, New York 10019

1 Mr. V. Boatwright, Jr.
R & D Manager
Electric Boat Division
General Dynamics Corporation
Groton, Conn. 06340

1 Gibbs & Cox, Inc.
21 West Street
New York, New York 10006
Attn: Technical Info. Control

1 Hydronautics, Inc.
Pindell School Road
Howard County
Laurel, Maryland 20810
Attn: Library

2 McDonnell Douglas Aircraft Co.
3855 Lakewood Blvd.
Long Beach, CA 90801
Attn: J. Hess
A.M.O. Smith

1 Lockheed Missiles & Space Co.
P.O. Box 504
Sunnyvale, CA 94088
Attn: Mr. R.L. Waid, Dept. 57-74
Bldg. 150, Facility 1

1 Newport News Shipbuilding & Dry
Dock Company
4101 Washington Avenue
Newport News, Virginia 23607
Attn: Technical Library Dept.

1 North American Aviation, Inc.
Space & Information Systems Div.
12214 Lakewood Blvd.
Downey, CA 90241
Attn: Mr. Ben Ujihara (SL-20)

1 Nielsen Engineering & Research, Inc.
850 Maude Avenue
Mountain View, CA 94040
Attn: Mr. S.B. Spangler

1 Oceanics, Inc.
Technical Industrial Park
Plainveiw, L.I., New York 11803

1 Society of Naval Architects
and Marine Engineers
74 Trinity Place
New York, New York 10006
Attn: Technical Library

1 Sun Shipbuilding & Dry Dock Co.
Chester, Penna 19000'
Attn: Chief Naval Architect

1 Sperry Systems Management Division
Sperry Rand Corporation
Great Neck, New York 11020
Attn: Technical Library

1 Stanford Research Institute
Menlo Park, CA 94025
Attn: Library G-021

2 Southwest Research Institute
P.O. Drawer 28510
San Antonio, Texas 78284
Attn: Applied Mechanics Review
Dr. H. Abramson

1 Tracor, Inc.
6500 Tracor Lane
Austin, Texas 78721

1 Mr. Robert Taggart
3930 Walnut Street
Fairfax, Virginia 22030

1 Ocean Engr. Department
Woods Hole Oceanographic Inst.
Woods Hole, Mass. 02543

1 Worcester Polytechnic Inst.
Alden Research Laboratories
Worcester, Mass. 01609
Attn: Technical Library

1 Applied Physics Laboratory
University of Washington
1013 N. E. 40th Street
Seattle, Washington 98105
Attn: Technical Library

1 University of Bridgeport
Bridgeport, Conn. 06602
Attn: Dr. E. Uram

1 Cornell University
Graduate School of Aerospace Engr.
Ithaca, New York 14850
Attn: Prof. W.R. Sears

4 University of California
Naval Architecture Department
College of Engineering
Berkeley, CA 94720
Attn: Library
Prof. W. Webster
Prof. J. Paulling
Prof. J. Wehausen

3 California Institute of Technology
Pasadena, CA 91109
Attn: Aeronautics Library
Dr. T.Y. Wu
Dr. A.J. Acosta

1 Docs/Repts/Trans Section
Scripps Institution of
Oceanography Library
University of California, San Diego
P.O. Box 2367
La Jolla, CA 92037

1 Catholic University of America
Washington, D.C. 20017
Attn: Dr. S. Heller, Dept. of
of Civil & Mech. Engr.

1 Colorado State University
Foothills Campus
Fort Collins, Colorado 80521
Attn: Reading Room, Engr. Res. Center

1 University of Calif. at San Diego
La Jolla, CA 92038
Attn: Dr. A.T. Ellis
Dept. of Applied Math

2 Flordia Atlantic University
Ocean Engineering Department
Boca Raton, Fla 33432
Attn: Technical Library
Dr. S. Dunne

2 Harvard University
Pierce Hall
Cambridge, Mass 02138
Attn: Prof. G. Carrier
Gordon McKay Library

1 University of Hawaii
Department of Ocean Engineering
2565 The Mall
Honolulu, Hawaii 96822
Attn: Dr. C. Bretschneider

1 University of Illinois
Urbana, Illinois 61801
Attn: Dr. J. Robertson

3 Institute of Hydraulic Research
The University of Iowa
Iowa City, Iowa 52241
Attn: Library
Dr. L. Landweber
Dr. J. Kennedy

1 The John Hopkins University
Baltimore, Md. 21218
Attn: Prof. O. Phillips
Mechanics Depts.

1 Kansas State University
Engineering Experiment Station
Seaton Hall
Manhattan, Kansas 66502
Attn: Prof. D. Nesmith

1 University of Kansas
Chm. Civil Engr. Dept. Library
Lawrence, Kansas 66044

1 Fritz Engr. Laboratory Library
Depart. of Civil Engr.
Lehigh University
Bethlehem, Penna 18015

5 Department of Ocean Engineering
Massachusetts Inst. of Technology
Cambridge, Mass. 02139
Attn: Department Library
Prof. P. Leehey,
Profs. M. Abkowitz , P. Mandel
Dr. J. Newman

1 Parsons Laboratory
Massachusetts Institute of Technology
Cambridge, Mass 02139
Attn: Prof. A. Ippen

5 St. Anthony Falls Hydr. Laboratory
University of Minnesota
Mississippi River at 3rd Ave., S.E.
Minneapolis, Minn. 55414
Attn: Director
Mr. J. Wetzel
Mr. F. Schiebe
Mr. J. Killen
Dr. C. Song

3 Department of Naval Architecture
and Marine Engineering
University of Michigan
Ann Arbor, Michigan 48104
Attn: Library
Dr. T.F. Ogilvie
Prof. F. Hammitt

2 College of Engineering
University of Notre Dame
Notre Dame, Indiana 46556
Attn: Engineering Library
Dr. A. Strandhagen

2 New York University
Courant Inst. of Math. Sciences
251 Mercier Street
New York, New York 10012
Attn: Prof. A. Peters
Prof. J. Stoker

New York University
University Heights
Bronx, New York 10453
Attn: Prof. W. Pierson, Jr.

Department of Aerospace and
Mechanical Sciences
Princeton University
Princeton, New Jersey 08540
Attn: Prof. G. Mellor

3 Davidson Lab
Stevens Institute of Technology
711 Hudson Street
Hoboken, New Jersey 07030
Attn: Library
Mr. J. Breslin
Mr. S. Tsakonas

1 Department of Mathematics
St. John's University
Jamaica, New YORK 11432
Attn: Prof. J. Lurye

1 Applied Research Lab Library
University of Texas
P.O. Box 8029
Austin, Texas 78712

College of Engineering
Utah state University
Logan, Utah 84321
Attn: Dr. R. Jeppson

2 Stanford University
Stanford, CA 94305
Attn: Engineering Library
Dr. R. Street

3 Webb Institute of Naval Architecture
Crescent Beach Road
Glen Cover, L.I., New York 11542
Attn: Library
Prof. E.V. Lewis
Prof. L.W. Ward

1 National Science Foundation
Engineering Division Library
1800 G Street N.W.
Washington, D.C. 20550

1 University of Connecticut
Box U-37
Storrs, Conn. 06268
Attn: Dr. V. Scottron
Hydraulic Res. Lab

Long Island University
Graduate Department of
Marine Science
40 Merrick Avenue
East Meadow, L.I., N.Y. 11554
Attn: Prof. David Price

1 Dr. Douglas E. Humphreys (Code 712)
Naval Coastal Systems Lab
Panama City, Florida 32401

Unclassified

Security Classification

DOCUMENT CONTROL DATA - R & D

Security classification of title, body of abstract and indexing annotation must be entered when the overall report is classified

1. ORIGINATING ACTIVITY (Corporate author) Institute of Hydraulic Research The University of Iowa	2a. REPORT SECURITY CLASSIFICATION Unclassified 2b. GROUP

3. REPORT TITLE

An Experimental Study of the Thick Turbulent Boundary Layer Near the Tail of a Body of Revolution

4. DESCRIPTIVE NOTES (*Type of report and inclusive dates*)

IIHR Report No. 142

5. AUTHOR(S) (*First name, middle initial, last name*)

V.C. Patel, A. Nakayama and R. Damian

6. REPORT DATE	7a. TOTAL NO. OF PAGES	7b. NO. OF REFS
January 1973	51	15

8a. CONTRACT OR GRANT NO.	9a. ORIGINATOR'S REPORT NUMBER(S)
N00014-68-A-0196-0002 b. PROJECT NO.	IIHR Report No. 142
	9b. OTHER REPORT NO(S) (*Any other numbers that may be assigned this report*)

10. DISTRIBUTION STATEMENT

Approved for public release; distribution unlimited

11. SUPPLEMENTARY NOTES	12. SPONSORING MILITARY ACTIVITY
	Naval Ship Research and Development Center

13. ABSTRACT

Detailed measurements of pressure distributions, mean velocity profiles and Reynolds stresses were made in the thick incompressible axisymmetric turbulent boundary layer near the tail of a body of revolution. The results indicate a number of important differences between the behavior of a thick and a thin boundary layer. The thick boundary layer is characterized by significant variations of static pressure across it and an abnormally low level of turbulence. The static pressure variation is associated with a strong interaction between the boundary layer and the potential flow outside it, while the changes in the turbulence structure appear to be a consequence of the transverse surface curvature. In order to predict the behavior of the flow in the tail region of a body of revolution it is not therefore possible to use conventional thin-boundary-layer calculation procedures.

DD FORM 1473 (PAGE 1)

KEY WORDS	LINK A		LINK B		LINK C	
	ROLE	WT	ROLE	WT	ROLE	WT
Turbulent boundary layers						
Axisymmetric flow						
Transverse curvature						
Measurements						
Velocity profiles						
Reynolds stresses						
Static-pressure variations						
Interaction						